Theses and Dissertations

1986

Nitrogen implanted polycrystalline silicon resistors /

Carl Alexis Peridier
Lehigh University

Follow this and additional works at: https://preserve.lehigh.edu/etd

 Part of the Electrical and Computer Engineering Commons

NITROGEN IMPLANTED POLYCRYSTALLINE

SILICON RESISTORS

by

Carl Alexis Peridier

A Thesis

Presented to the Graduate Committee

of Lehigh University

in Candidacy for the Degree of

Master of Science

in

Electrical Engineering

Lehigh University

1986

This thesis is accepted and approved in partial fulfillment of the requirements for the degree of Master of Science.

Sept. 12, 1986
(date)

Frank H. Hielscher
Professor in Charge

Lawrence J. Varnerin
Chairman of Department

ACKNOWLEDGMENTS

TABLE OF CONTENTS

LIST OF TABLES

LIST OF FIGURES

ABSTRACT

Nitrogen implanted polycrystalline silicon resistors were studied as an alternative to As, B or P doped polysilicon resistors in order to obtain better resistivity control with implant dose variations in integrated circuit manufacturing. The variation in resistivity and activation energy with implant dose were found to be much smaller for N doped polysilicon resistors than those reported for As, B or P doped resistors. The measured resistivity values ranged from 7.93E5 Ohm-cm at a N dopant density of $1.24E20/cm^3$ to 2.72E4 Ohm-cm at $3.92E21/cm^3$ of N, with an increase to 4.34E4 Ohm-cm at $4.71E21/cm^3$, the highest concentration. The activation energy ranged from half bandgap for lightly doped samples to 0.36eV for heavily doped samples. The I-V characteristics follow the same hyperbolic sine relationship as for polycrystalline silicon resistors with normal dopants, from 25^oC to 110^oC, and deviate from this at 150^oC. The effects of 1000^oC and 1100^oC anneals for 30 min were studied and the results were affected by diffusion from the heavily As doped polysilicon contacts. Manufacturing with N implanted polysilicon resistors will be limited, due to the very high implant doses required.

1

Chapter I

Introduction

Polycrystalline silicon (polysilicon) resistors are commonly used as load elements in integrated circuits due to the high value of resistance obtainable in a small amount of area. To control the value of resistors, polysilicon is usually lightly doped with As, B or P. Unfortunately, the value of resistance changes about 5 orders of magnitude over a change in dopant concentration of 2 orders of magnitude in the lightly doped region [1-16] which causes problems of reproducibility during manufacture where implant doses have a spread in concentration.

Implanted nitrogen acts as a weak n-type dopant in crystalline silicon. Only a small fraction of the implanted nitrogen atoms become electrically active. The percent of electrically active dopants is concentration dependent, peaking at about 0.6% for a dose of $10^{17} cm^{-3}$. An actual decrease in the carrier concentrations occurs at higher implant doses [17]. With these properties, nitrogen therefore may offer better control of resistor values than the more commonly used dopants.

This thesis presents a study of nitrogen implanted polysilicon resistors. A previous measurement of polysilicon resistivity versus

2

nitrogen dopant concentration was made by H. Hayashi, H. Yamoto and T. Oshime from the SONY Corporation [18]. This thesis verifies their results and expands on them by also measuring the length dependence, temperature effects, current voltage relationships, post anneal effects and grain sizes.

A review of the current theoretical and experimental work with As, B and P doped polysilicon resistors is given and compared to the results of this study.

It was found that, as expected, the resistance value is more weakly dependent on the nitrogen concentration than normal dopants. There is a variation in resistivity with dopant concentration by a factor of 30 instead of 100,000 and the resistance starts to increase at higher dopant levels. This is comparable with the measurements of Hayashi [18].

The length and I-V relationships are similar to resistors with normal dopants. The resistance is linear with resistor length over a range of 3.9 to 22.9 μm, and the I-V curves follow the hyperbolic sine relationship found on normally doped polysilicon resistors [4,6-10,11,19,20].

Resistance values follow the Arrhenius relationship with temperature

Chapter I

Introduction

Polycrystalline silicon (polysilicon) resistors are commonly used as load elements in integrated circuits due to the high value of resistance obtainable in a small amount of area. To control the value of resistors, polysilicon is usually lightly doped with As, B or P. Unfortunately, the value of resistance changes about 5 orders of magnitude over a change in dopant concentration of 2 orders of magnitude in the lightly doped region [1-16] which causes problems of reproducibility during manufacture where implant doses have a spread in concentration.

Implanted nitrogen acts as a weak n-type dopant in crystalline silicon. Only a small fraction of the implanted nitrogen atoms become electrically active. The percent of electrically active dopants is concentration dependent, peaking at about 0.6% for a dose of $10^{17} cm^{-3}$. An actual decrease in the carrier concentrations occurs at higher implant doses [17]. With these properties, nitrogen therefore may offer better control of resistor values than the more commonly used dopants.

This thesis presents a study of nitrogen implanted polysilicon resistors. A previous measurement of polysilicon resistivity versus

nitrogen dopant concentration was made by H. Hayashi, H. Yamoto and T. Oshime from the SONY Corporation [18]. This thesis verifies their results and expands on them by also measuring the length dependence, temperature effects, current voltage relationships, post anneal effects and grain sizes.

A review of the current theoretical and experimental work with As, B and P doped polysilicon resistors is given and compared to the results of this study.

It was found that, as expected, the resistance value is more weakly dependent on the nitrogen concentration than normal dopants. There is a variation in resistivity with dopant concentration by a factor of 30 instead of 100,000 and the resistance starts to increase at higher dopant levels. This is comparable with the measurements of Hayashi [18].

The length and I-V relationships are similar to resistors with normal dopants. The resistance is linear with resistor length over a range of 3.9 to 22.9 μm, and the I-V curves follow the hyperbolic sine relationship found on normally doped polysilicon resistors [4,6-10,11,19,20].

Resistance values follow the Arrhenius relationship with temperature

and the activation energy is less variable with implant dose and higher than resistors with normal dopants. The activation energy for N doped polysilicon ranges from about 0.55 eV to 0.36 eV whereas for normal dopants it ranges as low as 0.06 eV [2,7,19]. These resistors are relatively insensitive to annealing. After a 30 min $1000^\circ C$ anneal, there was little change in resistance.

For practical applications, nitrogen doped polysilicon has a number of desirable attributes. The main drawback with nitrogen implanted resistors, however, is that the implant doses required are very high and consequently the implant time may be very long which would prohibit cost effective manufacturing unless there were higher current implant machines available. Until these are available, this process cannot be recommended for commercial manufacturing.

Chapter II

Theory and Previous Experimental Results

Lightly doped polysilicon resistors have been an area of consider-
able interest since the early 1970's, when they started to be con-
sidered for load elements in integrated circuits. A significant
body of literature exists on the conduction mechanisms of polysili-
con doped with As, P and B, much of which was published recently.

It is possible to increase the resistivity of polysilicon by adding
oxygen during the deposition process, forming a semi-insulating
polycrystalline silicon film called SIPOS [21-24]. It has been
studied primarily as a passivation layer to replace SiO_2 in inte-
grated circuits. The resistivity increases due to SiO_2 growth at
the grain boundaries [24], increasing the resistivity by a factor of
1000 with an increase in the atomic weight percent of oxygen from 0%
to 30% . Above 45% the material is amorphous. The film is ohmic
over a large voltage range [22,23]. The reproducibility of these
films is difficult to control and generally a resistivity slightly
lower than undoped polysilicon is desired. Consequently SIPOS has
not been used as a high value resistor material in integrated cir-
cuits.

One of the dominant characteristics of doped polysilicon, and one of

its main problems for integrated circuit manufacturing, is the drop in resistivity of about 5 orders of magnitude over a change in dopant concentration of 2 orders of magnitude, which makes precise control of its value difficult. The use of nitrogen as a dopant is proposed as a solution to this problem.

There exists very little literature on nitrogen doped polysilicon. Therefore a review of the literature on common dopants in polysilicon, then nitrogen as a dopant in crystalline silicon, and then one article on nitrogen as a dopant in polysilicon as well as some other articles on nitrogen as a passivator in polysilicon will be presented.

A. As, B, P in Polysilicon

Polysilicon is composed of small crystallites, joined together by grain boundaries. These grain boundaries are layers of disordered atoms which separate adjacent crystallites of different orientations [25]. One of the initial explanations for the abrupt change in resistivity versus dopant concentration was attributed to dopant segregation at the grain boundaries [3]. The dopant atoms were assumed to diffuse to the grain boundary regions where they became electrically inactive. As the concentrations are increased, the grain boundaries become saturated and the additional dopants are then incorporated into the crystallites where they become electrically active, lowering the resistivity. This theory could not,

6

however, explain the observed mobility minimum at a certain doping level, or the temperature dependence of the resistivity.

A second explanation was developed which explains the conduction mechanisms of polysilicon by carrier trapping in the grain boundaries [15]. Since the grain boundaries are disordered, there are a large number of defects which results in a large number of trapping states. These traps reduce the number of free carriers and also become electrically charged which creates a potential barrier which impedes the flow of carriers from one crystallite to another, reducing the mobility. This theory has been successful in explaining most of the conduction mechanisms of polysilicon.

There are cases where actual dopant segregation to the grain boundaries occurs [26,27]. This results in a resistivity dependence on the dopant species and changes in resistivity upon annealing, which cannot be explained by the carrier trapping model alone. Both arsenic and phosphorus have a strong tendency to segregate to the grain boundaries, although boron does not. Phosphorus segregation is also used to explain the variation in the calculated grain size from the carrier trapping theory with changes in temperature [27]. The conduction mechanism in these cases is still dominated by carrier trapping.

A.1 Conductivity

The basic carrier trapping model, as explained by Seto [15], is summarized below. This particular model is discussed because it is used in most of the literature on lightly doped polysilicon resistors. Some of the derivations are carried out in order to highlight an error in Seto's work.

To simplify the model, polysilicon is assumed to be a linear array of crystallites of size L (see Fig. 2.1) and the dopant is uniformly distributed with a concentration N. The grain boundary is assumed to contain a surface density of traps Q_t with an energy E_t with respect to the Fermi level. These traps are neutral until they hold a charged carrier. The trapping of carriers at the grain boundary creates a depletion region on either side of the grain boundary of width $L/2 - \ell$ (see Fig. 2.1b).

Using Poisson's equation

$$\frac{d^2V}{dx^2} = \frac{qN}{\epsilon}$$

for $\ell < |x| < L/2$

Solving, using dV/dx is zero at $x = \ell$ gives

$$V(x) = (qN/2\epsilon)(x-\ell)^2 + V_o \qquad (2)$$

for $\ell < |x| < L/2$, where V_o is the energy of the valence band.

Note that the notation is unusual in that the intrinsic Fermi level is at zero energy, with the positive energy towards the valence

8

(a) Crystal Structure

(b) Charge Distribution

(c) Energy Band Structure
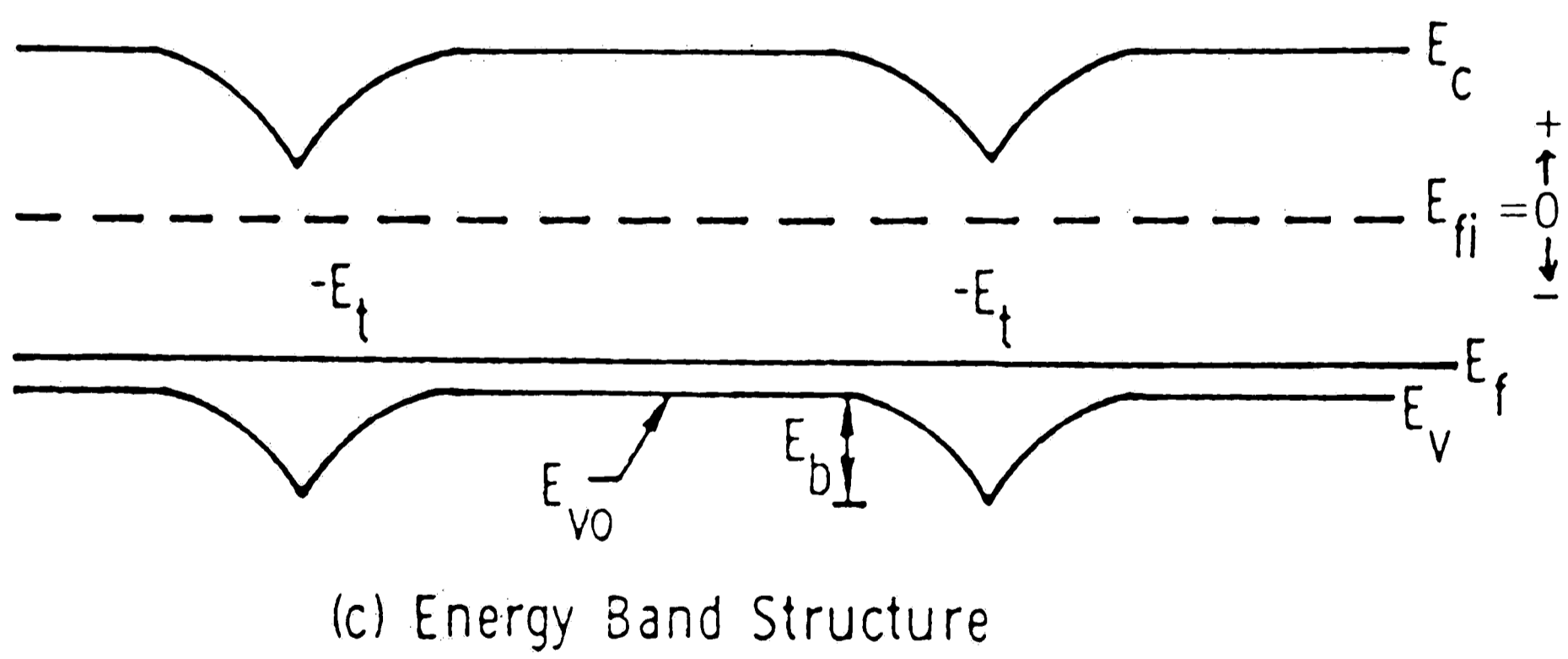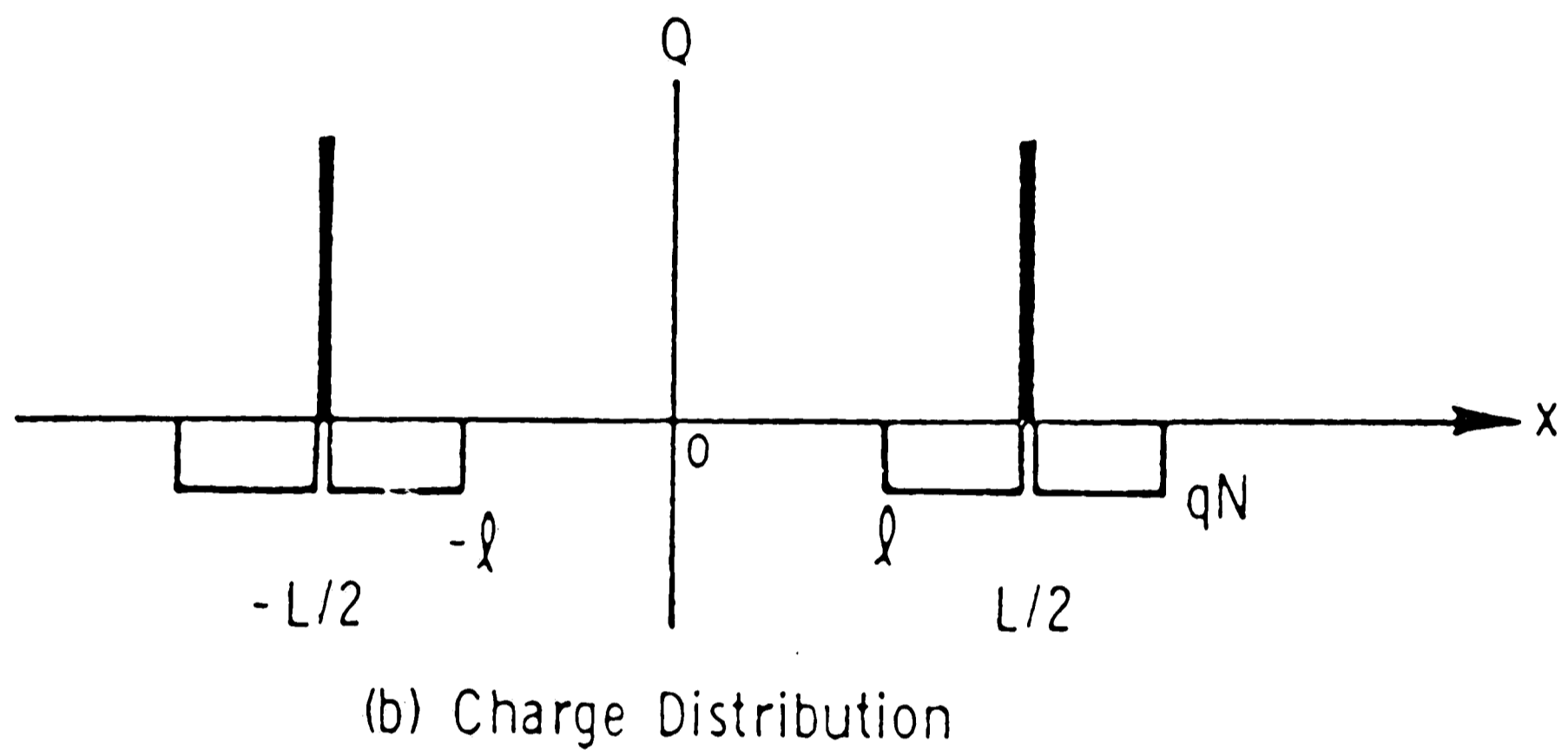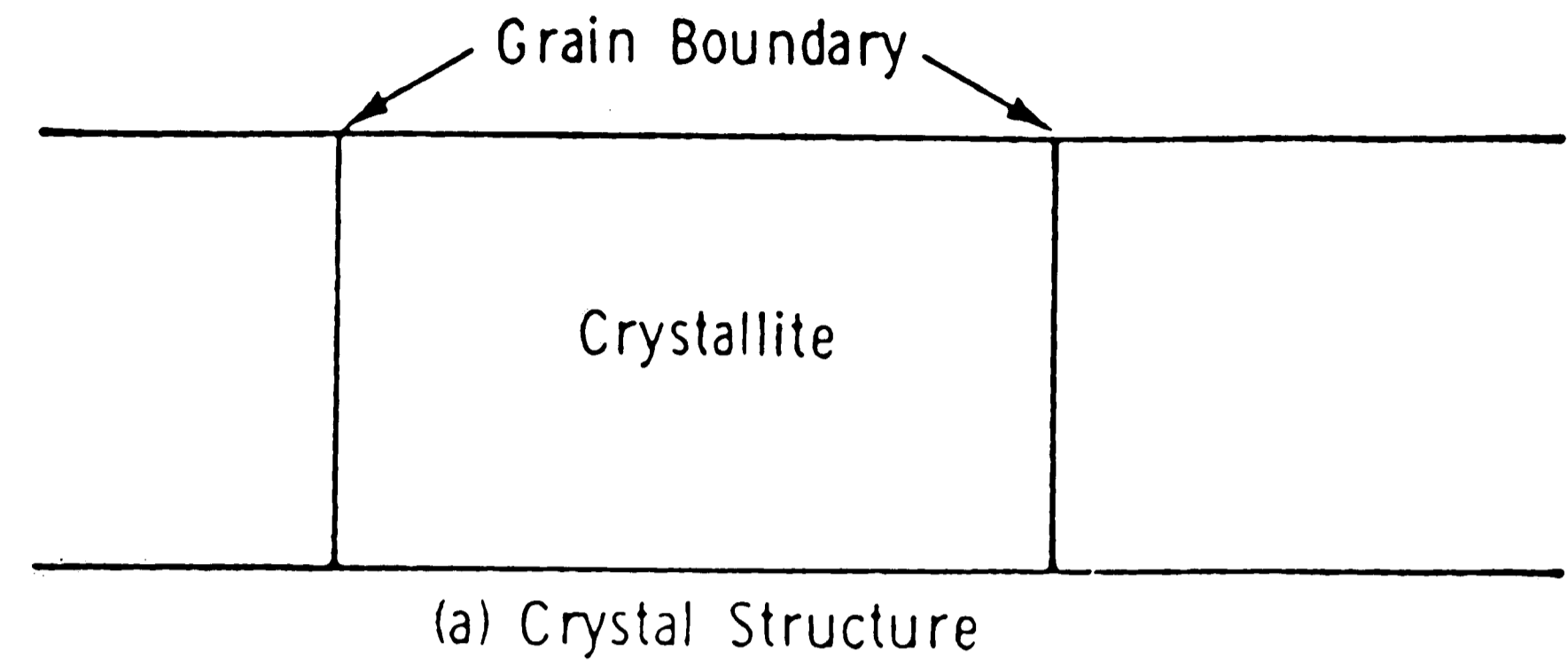
Fig. 2.1 Polysilicon Model (a) crystal structure, (b) charge distribution, (c) energy band structure from ref. 15.

band, see the band diagram in Fig. 2.1c.

For a given L and N, the crystal may be completely depleted: $LN < Q_t$, or only partially depleted: $LN > Q_t$. In the completely depleted case, where $LN < Q_t$, we have $\ell = 0$, so that equation (2) is

$$V(x) = V_o + (qN/2\epsilon)x^2, \quad |x| \leq L/2 \tag{3}$$

The barrier height, V_B, is the difference in potentials at $x = 0$ and $x = L/2$

$$V_B = qL^2N/8\epsilon \tag{4}$$

The carrier concentration at a given location is therefore

$$p(x) = N_v \exp\left\{[E_f - qV(x)]/kT\right\} \tag{5}$$

where N_v is the density of states and E_f is the Fermi level. The average carrier concentration, p_a, is derived by integrating equation (5) from $-L/2$ to $L/2$ and dividing by L.

$$p_a = \frac{1}{L} \int_{-L/2}^{L/2} p(x)\, dx$$

$$= (N_v/L)\exp[(E_f - qV_o)/kT] \int_{-L/2}^{L/2} \exp[-(q^2N/2\epsilon kT)x^2]\,dx \tag{6}$$

Using $\int_{-x}^{x} \exp(-t^2/2)dt = \sqrt{2\pi}\, \mathrm{erf}(x/\sqrt{2})$

$$p_a = (N_v/L)\exp[(E_f - qV_o)/kT](2\pi\epsilon\, kT/q^2N)^{1/2} *$$
$$\mathrm{erf}[(qL/2)(N/2\epsilon kT)^{1/2}] \tag{7}$$

Substituting

$$n_i = N_v \exp(-E_g/2kT)$$

10

and note that $qV_o = E_g/2$ using Seto's notation:

$$p_a = (n_i/Lq)(2\pi\epsilon kT/N)^{1/2}\exp(E_f/kT)*erf[(qL/2)(N/2\epsilon kT)^{1/2}] \quad (8)$$

In Seto's derivation at this point there remains an extra factor of $\exp(E_B/kT)$ in the above equation (equation (8) in ref.[15]). This error is carried in his subsequent derivations, although if the calculations are carried out with the numbers used in his graphs, it appears that this extra factor was omitted for his calculations.

The Fermi level is determined by equating the number of carriers trapped to the total number of occupied states:

$$LN = \frac{Q_t}{2\exp[(E_t-E_f)/kT]+1}$$

The Fermi level is solved for

$$E_f = E_t - kT\ln[(Q_t/LN - 1)/2] \quad (9)$$

With the above information, and if L, Q_t and E_t are known, the carrier concentrations vs doping densities can be calculated for $LN<Q_t$.

At larger doping concentrations, where $LN>Q_t$, only part of the crystallite is depleted and $\ell>0$. The barrier height is, from eq. (2)

$$V_B = qQ_t^2/8\epsilon N \quad (10)$$

Using this and eq. (4), the barrier height versus doping concentration can be determined and is pictured in Fig. 2.2. As the doping concentration is increased, the barrier height rises linearly with N

11
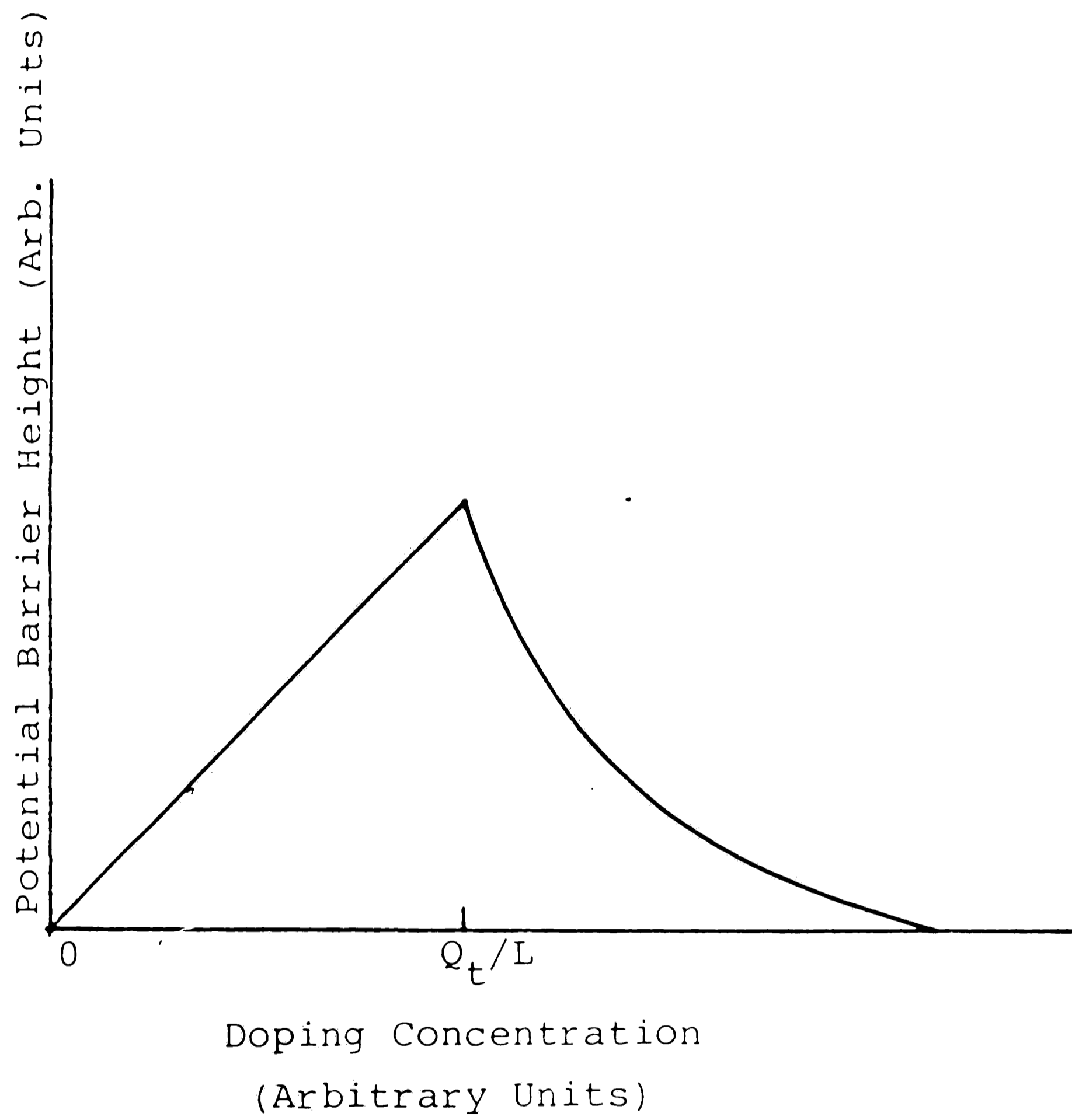
Fig. 2.2 Barrier Height vs Doping Concentration
from ref. 15.

until it reaches its maximum at $LN=Q_t$. At this point all of the interface traps are filled. Then the crystallite is no longer completely depleted and the barrier height decreases as $1/N$ and the dipole layer is narrowed as the concentration is increased. It will be found that the mobility is exponentially dependent on the barrier height and therefore reaches a minimum at the transition point $LN=Q_t$.

For the case where $LN>Q_t$, the concentration in the undepleted region is

$$p_b= N_v \exp[(E_f-E_v)/kT] = N$$

and the average carrier is

$$p_a= p_b[(1-Q_t/LN)+(1/qL)(2\epsilon\%kT/N)^{1/2}*erf[(qQ_t/2)(1/2\epsilon\%kTN)^{1/2}]$$

$$(11)$$

Assuming that the resistivity in the single crystal region is much lower than that through the grain boundary region, this is the only region considered. The two conduction mechanisms through the grain boundary are thermionic emission and tunneling (field emission). Since the barrier height and width for polysilicon increase together, and tunneling dominates for high and narrow barriers, only thermionic emission is considered.

The thermionic emission current density, J_{th} for an applied voltage V_a is

13

$$J_{th} = qp_a(kT/2\pi m^*)^{1/2}\exp(-qV_B/kT)[\exp(qV_a/kT)-1] \qquad (12)$$

where m^* is the carrier effective mass. This equation is valid only

for $qV_B > kT$.

For a small voltage drop across the grain boundary, the above equation can be expanded to

$$J_{th} = q^2 p_a(1/2\pi m^* kT)^{1/2}\exp(-qV_B/kT)V_a \qquad (13)$$

for $V_a \ll kT/q$

which is a linear current voltage relationship.

Using $J = \sigma E = \sigma V_a/L$, the conductivity of a polysilicon film of grain

size L is

$$\sigma = Lq^2 p_a(1/2\pi m^* kT)^{1/2}\exp(-qV_B/kT) \qquad (14)$$

Using the fact that the mobility is related to the conductivity via:

$$\sigma = qp\mu$$

we see that

$$\mu = Lq(2\pi m^* kT)^{-1/2}\exp(-E_B/kT) \qquad (15)$$

As shown in Fig. 2.2, the energy barrier reaches a maximum as a

function of doping at $LN = Q$ and therefore the mobility is at a mini-

mum at this point.

For $LN < Q_t$, substituting for p_a eq. (8), corrected from Seto's deri-

vation

$$\sigma = (n_i q)(\epsilon/Nm^*)^{1/2}\exp[(E_f-E_B)/kT]erf[(qL/2)(N/2\epsilon kT)^{1/2}]$$

Using eq. (9) for E_f

14

$$\exp(E_f/kT) = [\exp(E_t/kT)]\exp[-\ln(Q_t/LN -1)/2]$$

$$= \left(\frac{\exp(E_t/kT)}{(Q_t/LN - 1)/2} \right) \qquad (16)$$

The final form is

$$\sigma = \frac{n_i q(\epsilon/Nm^*)^{1/2} erf[(qL/2)(N/2\ kT)^{1/2}]\exp[(E_t-E_B)/kT]}{[(1/2)((Q_t/LN)-1)]} \qquad (17)$$

where $E_B = q^2L^2N/8\epsilon$ and $LN < Q_t$

The above equation gives the complete description of the conductivity variation with respect to the doping concentration and temperature for $LN < Q_t$.

For the case of $LN > Q_t$, using eqn's (10,11 and 14), the solution is

$$\sigma = Lq^2N\left\{ [1-(Q_t/LN)]+(1/qL)(2\epsilon kT\pi/N)^{1/2}* \right.$$

$$\left. erf[(qQ_t/2)(2\epsilon kTN)^{-1/2}\right\}*(2\pi m^* kT)^{-1/2}\exp(-q^2Q_t^2/8\epsilon NkT) \qquad (18)$$

The above two equations, derived using Seto's simple assumptions, account for most of the observed properties of lightly doped poly-silicon, with moderate grain sizes.

The temperature dependence of the conductivity may be simplified from the above equations. Using equation (16) for $LN < Q_t$, noting that

15

$$n_i = N_V \exp(-E_g/2kT)$$

and ignoring the $T^{3/2}$ temperature dependence of the effective

density of states N_V, gives

$$\sigma(T) \propto \exp[-(E_g/2 - E_f + E_B)/kT] \qquad (19)$$

For $LN > Q_t$, using eqns (11) and (14), we have

$$\sigma(T) \propto \exp(-E_B/kT) \qquad (20)$$

For undoped samples the activation energy for the conductivity is

$E_g/2 = 0.55$ eV. From the above two equations one can see that for

low doping concentrations, the activation energy is $E_g/2 - E_f + E_B$

and as the doping level is increased, it will lower to E_B.

A.2 Current Voltage Characteristics

A detailed calculation of the I-V characteristics of lightly doped

polysilicon resistors has been done by several other authors:

[4,7,11,16,20]. A common approach is to consider the grain boundary

as a Schottky barrier with thermionic emission of majority carriers.

The barrier is considered as a symmetrical semiconductor to semicon-

ductor junction. The conduction mechanism is thermionic emission,

using the requirement that $V_B > kT/q$. The net conduction across the

barrier is assumed to be the differences of the current fluxes in

the two directions. The current flux from right to left is [28]

$$J_1 = A^* T^2 \exp(-qV_{B0}/kT)[\exp(qV/kT)-1] \qquad (21)$$

where V_{B0} is the barrier height at zero bias ($E_c - E_f$ at the surface),

V is the applied voltage across the barrier, and A^* is the Richard-

son constant.

16

The current from left to right is

$$J_2 = A^* T^2 \exp(-qV_{B0}/kT)[\exp(-qV/kT)-1] \qquad (22)$$

The total current is the difference between J_1 and J_2, hence

$$J = J_1 - J_2 = 2A^* T^2 \exp(-qV_{B0}/kT)\sinh(qV/kT) \qquad (23)$$

The voltage drop across each barrier, V, can be expressed as the applied voltage across the resistor, V_a, and the number of grain boundaries along the length of the resistor, N_g, assuming that the voltage is divided equally on each side of the junctions, as

$$V = V_a/2N_g \qquad (24)$$

The result is

$$J = 2A^* T^2 \exp(-qV_{B0}/kT)\sinh(qV_a/2kTN_g) \qquad (25)$$

Here V_{B0} is equivalent to the barrier height mentioned earlier, which is a function of the dopant concentration.

B Previous Experimental Data

B.1 Resistivity vs. Dopant Concentration

Measurements of boron doped polysilicon resistors were made by Seto, in good agreement with his theory [15]. Fig. 2.3 shows the measured and theoretical calculations for the room temperature resistivity vs. doping concentration. The Hall mobility was measured vs. doping concentration (Fig. 2.4) and the mobility minimum can be seen which in turn results in a maximum in the barrier height. The average carrier concentration is shown in Fig.2.5. The specific details of the measurements depend strongly on the grain size of the polysili-

17
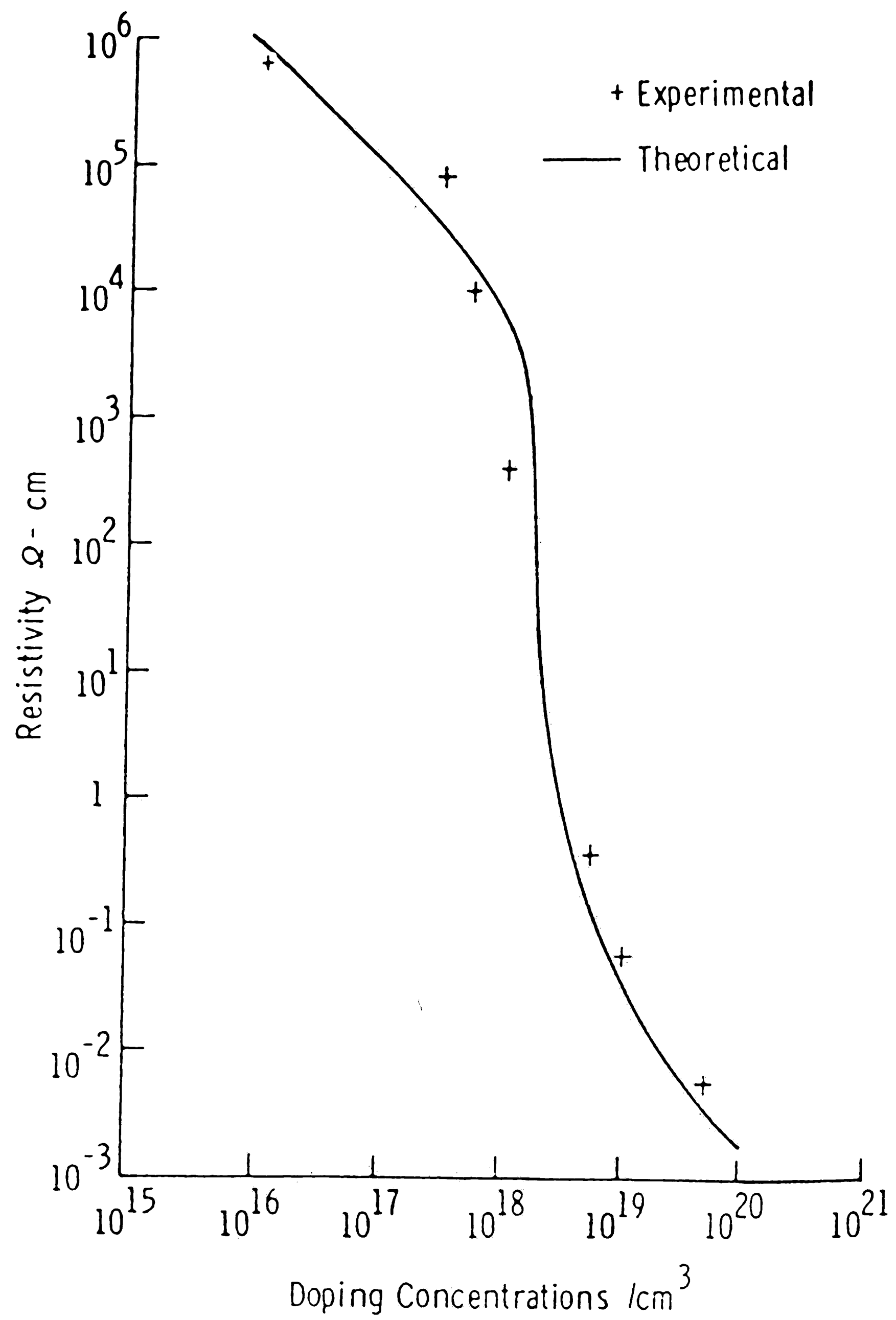
Fig. 2.3 Resistivity vs boron doping concentration (room temperature), from ref. 15.

18
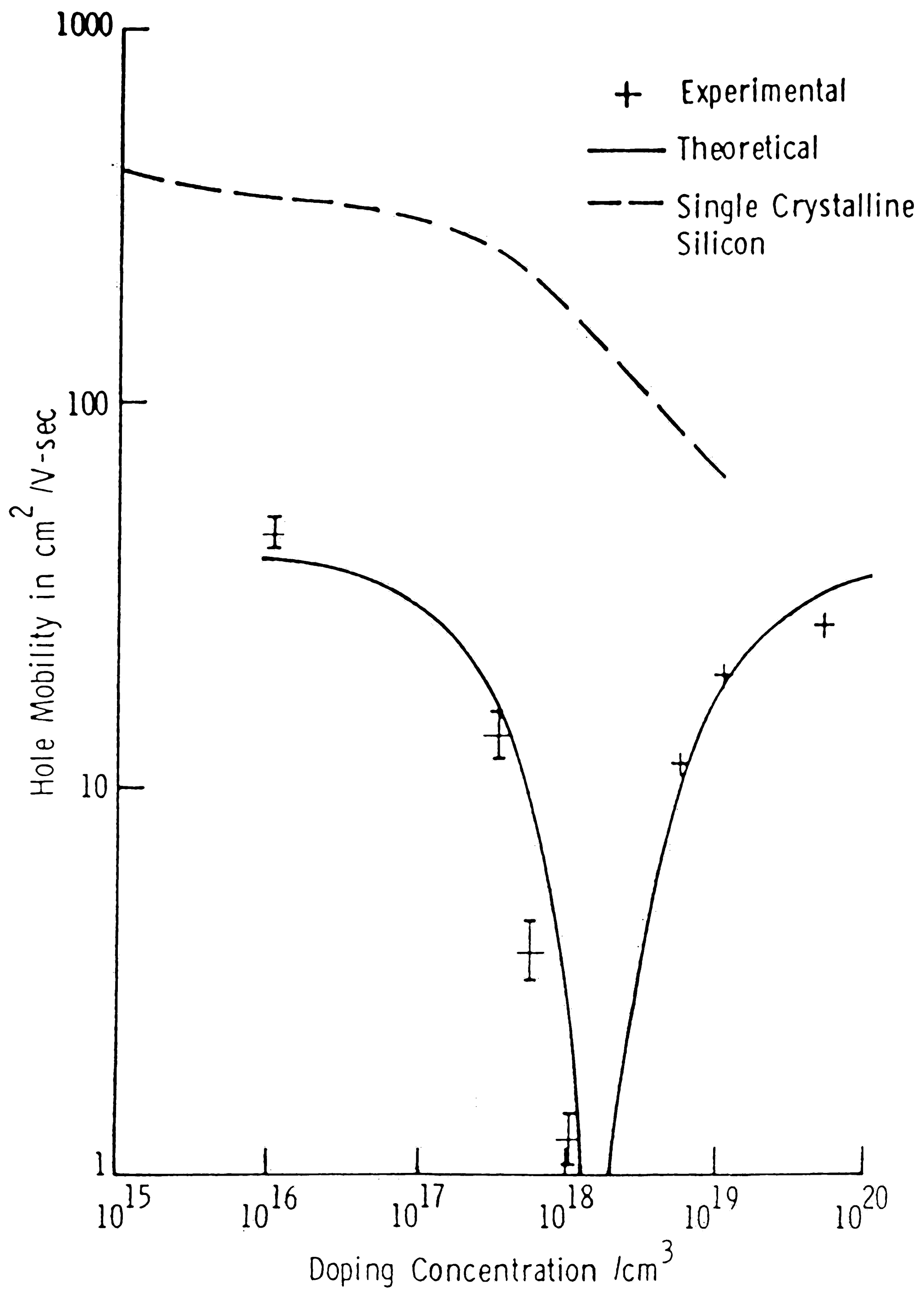
Fig. 2.4   Hall mobility vs boron doping concentration
(room temperature), from ref. 15.
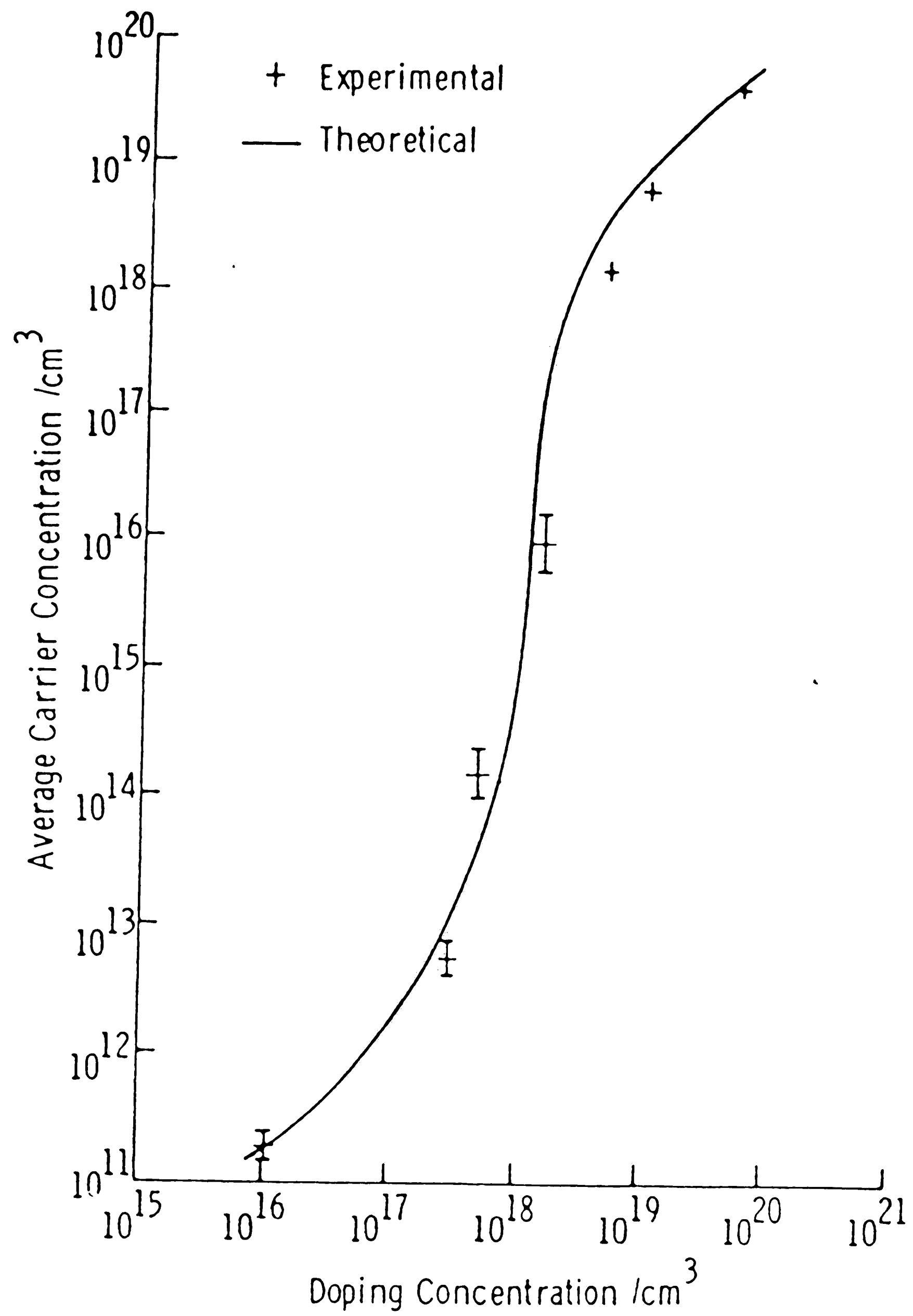
Fig. 2.5 Carrier concentration vs boron doping
concentration (room temperature), from ref. 15.

con and subsequent processing after doping. The results for each
experiment may vary from Seto's measurements but the basic proper-
ties remain the same.

Other measurements of R vs. N with various dopants have been done
by ref's. [1-8,10-14,16].

B.2 Activation Energy

The resistivity vs. temperature measurements follow the expected
Arrehenius relationship as in eqns (19 and 20), Fig. 2.6. The values
for the activation energy follow the expected curve of decreasing
from $E_g/2$ for low dopant concentrations to a low value for higher
concentration (Fig. 2.7). Other measurements were made by ref's.
[2,7,13,14,16].

B.3 Current Voltage Measurements

The derivation of the I-V characteristics results in the hyperbolic
sine relationship, eqn. (25).

$$I \propto \sinh(qV_a/2kTN_g)$$

which shows a good agreement with the data at and above room temper-
ature. An example of the agreement of this theory to the data is
given in Fig. 2.8. Other measurements can be found in ref's
[4,9,10,20].
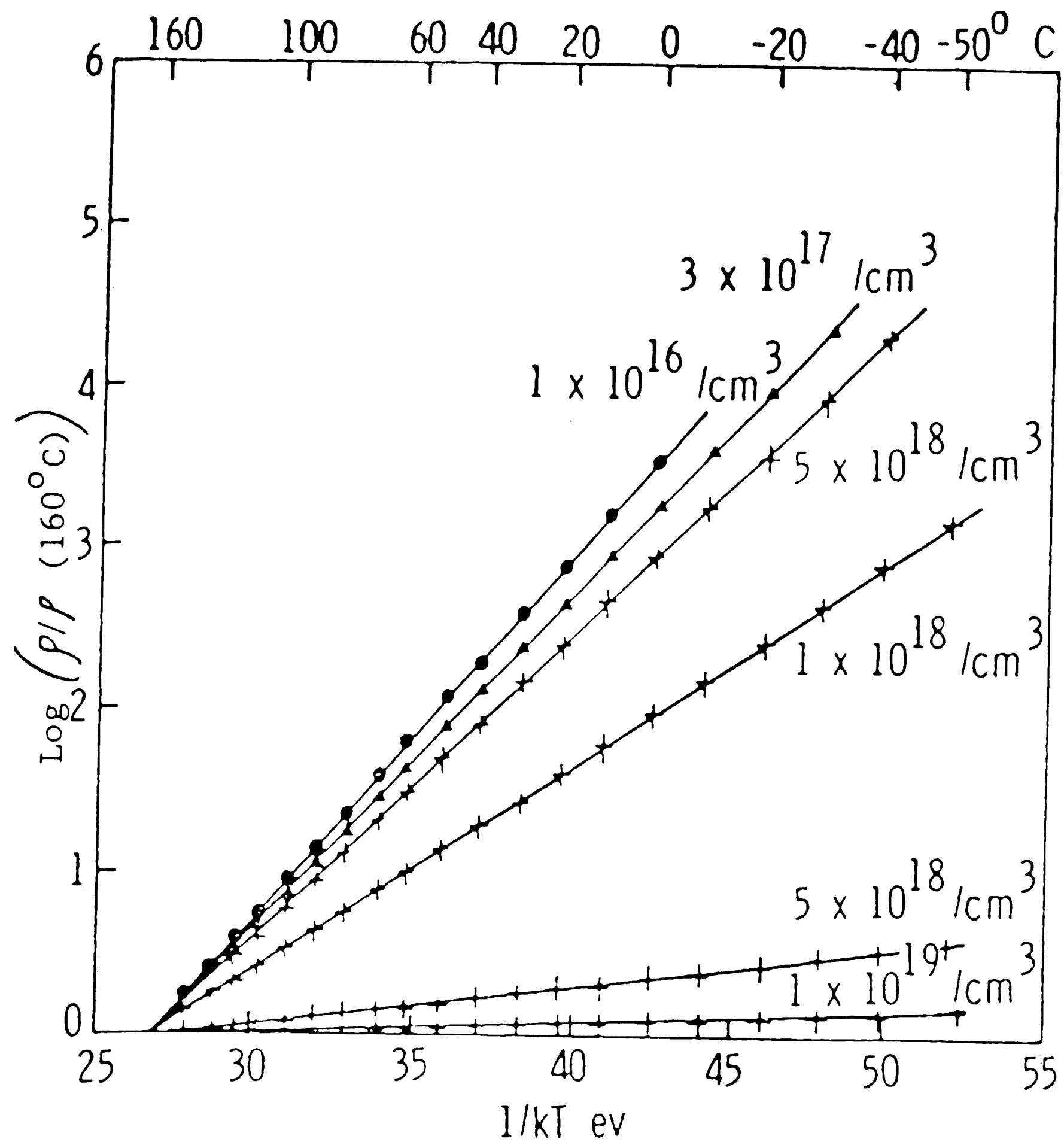
Fig. 2.6   Resistivity vs 1/kT, for different boron
doping concentrations, from ref. 15.
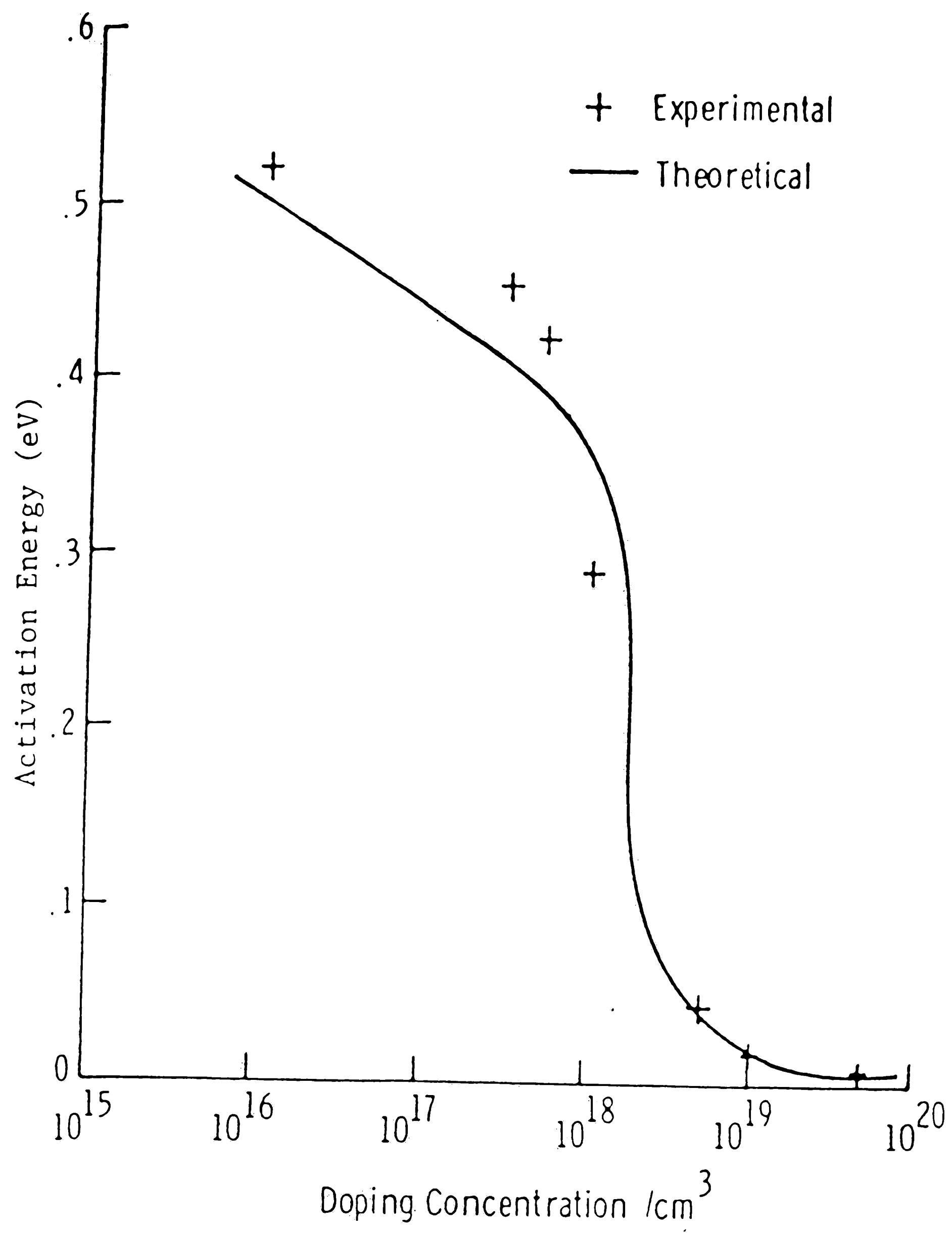
Fig. 2.7 Activation energy vs boron doping concentration, from ref. 15.

RECTANGULAR
RESISTORS OF
LENGTH 80μ, 120μ

●, ○ MEASURED
—— THEORY

$I = 1.98 \, \mathrm{SINH} \dfrac{V}{33.5}$

80μ 120μ

$I = 1.98 \, \mathrm{SINH} \dfrac{V}{49}$

$I = 2 I_S \, \mathrm{SINH} \dfrac{V}{2 N_g V_T}$

$I \approx I_S \dfrac{V}{N_g V_T}$

$I = \dfrac{2 N_g V_T}{R} \, \mathrm{SINH} \dfrac{V}{2 N_g V_T}$

ALL V
$\left(V_T = \dfrac{kT}{q} \right)$

$\dfrac{V}{N_g} \ll 2 V_T$

$R = \dfrac{V}{I}$

I (mA)

V (volts)
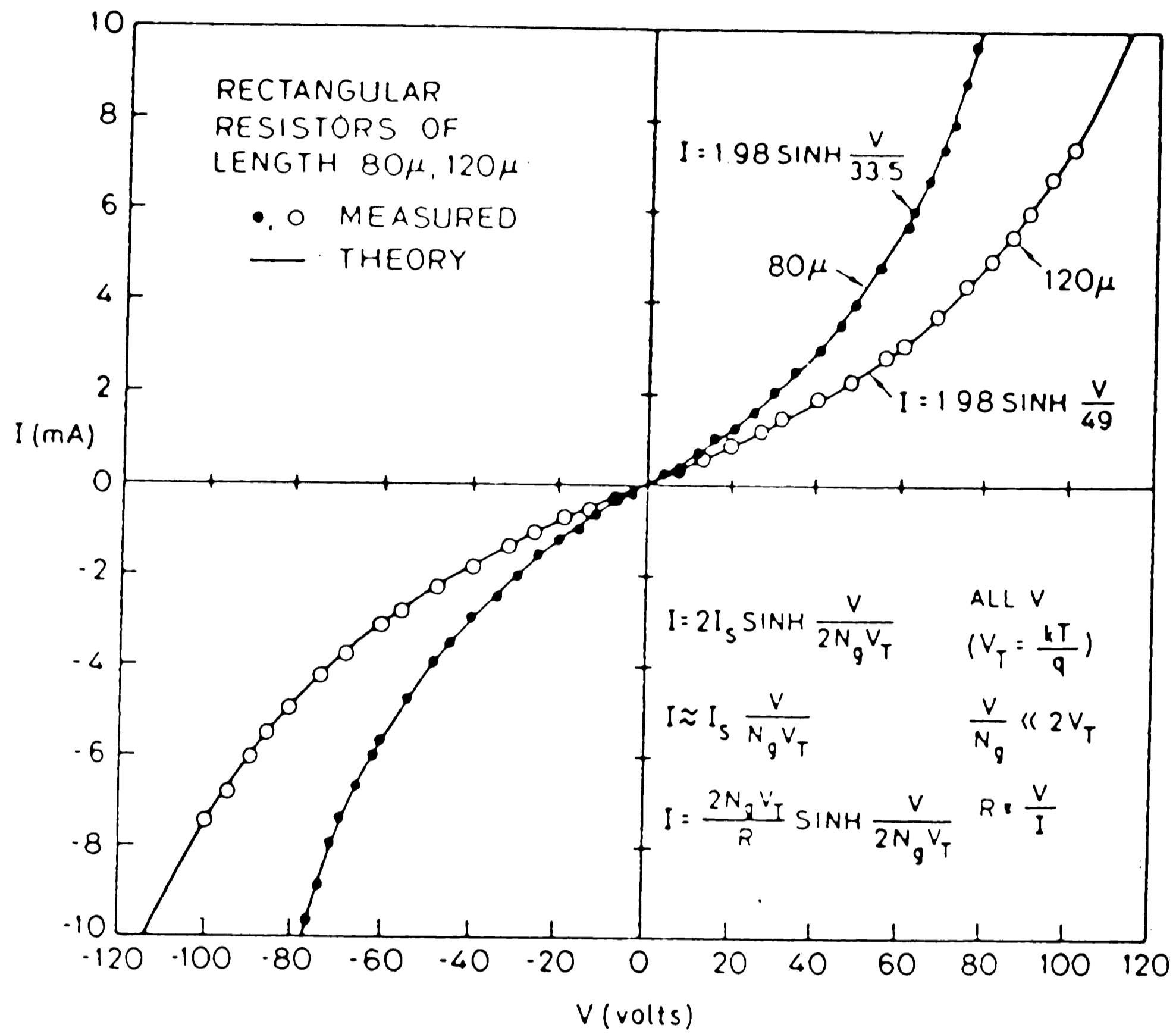
Fig. 2.8 Current voltage characteristics of boron
doped polysilicon, from ref. 7.

C. Further Refinements of the Theory

The above theory of Seto and Lu can explain most of the data under normal conditions of temperature, grain size and doping. Further refinements to the theory have been made by many authors to cover more extreme conditions.

C.1 Low Temperature

The simple theory of thermionic emission does not account for the data at low temperatures, and a theory including thermionic field emission at low temperatures has been developed by [4,6,10,27].

C.2 Amorphous Grain Boundary

Modifications of the simple theory have been done by treating the grain boundary as a nearly amorphous semiconductor [19], and traps are treated as a nonvanishing density of states in the band gap due to random potential fluctuations.

C.3 Undoped and Low Doped Polysilicon

The theory has been refined to account for undoped or lightly doped polysilicon. It is found that the hole current dominates in films of lightly doped polysilicon, even for donor-doped samples [13]. For undoped polysilicon, it is found that it is weakly p-type and the conduction mechanism looks like the avalanche breakdown of an n^+-i junction [29].

C.4 Growth and Anneal Effects

The polysilicon growth conditions, dopant species and concentration and the subsequent annealing conditions have a large effect on the electrical characteristics by changing the grain size, trapping state densities and dopant segregation. This has been studied by many authors [11,12,16,25,30-34]. These conditions and their electrical effects have been incorporated into a version of the processing simulation program SUPREM III [35].

D. Nitrogen in Single Crystal Silicon

The above theories and measurements were for the common dopants of As, B and P in polysilicon. The dopant N is uncommon for polysilicon resistors, but much research has been done on this element in crystalline silicon, which will now be reviewed.

Nitrogen acts as an unusual element in Si. While other Group V elements P, As, Sb and Bi act as typical shallow donors, N has an unusually weak influence on the electrical properties of crystalline Si. Doping of Si with N_2 gas or growing Si in its presence has no electrical effect. Nitrogen is often used as an inert ambient during Si processing, and commercial Si has dissolved N with no electrical effect [36]. Nitrogen doped single crystal Si is found to be mechanically stronger than pure Si [37]. One possible reason that there is no electrical activity with N_2 is that this molecule has a high dissociation energy (9.8eV) and is electrically neutral.

26

Nitrogen implanted into crystalline Si and then annealed shows donor characteristics [17,38,39,40]. The ionization level has been measured by several authors and the values range from 0.015 to 0.142 eV [17]. Some authors have detected double levels. New methods such as Electron Paramagnetic Resonance (EPR) have been used to measure the ionization level of substitutional N. Using this technique, K. L. Brower reported in earlier publications [41,42] a level for N of 0.58eV which he later reported was unsupported and unknown [43].

Only a small fraction of N atoms become electrically active, and this is dosage dependent, peaking at about 0.6% for a dose of $10^{17}/cm^3$ [17,44,45] for normal implant conditions. The carrier concentration is also dependent on the anneal temperature and peaks at $800^{\circ}C$. This decrease in the concentration above $800^{\circ}C$ is speculated to be due to the formation of N_2 or Si_3N_4, or due to evaporation [17]. Other measurements have shown that furnace annealing of N implanted Si above $1200^{\circ}C$ produces a buried layer of Si_3N_4 [46].

The solubility of N in liquid Si near the melting point has been measured as $10^{19}cm^{-3}$ [36] and $4.5\times10^{15}cm^{-3}$ for solid Si [17,47]. The diffusion coefficient for N in Si has been measured for implanted N as [17]

$$D = 0.87 \exp(-3.29/kT) cm^2/sec.$$

A comparison of these results with other elements in silicon is shown in Table 2.1.

E. Nitrogen in Polysilicon

As stated earlier, there is little research published on the subject of nitrogen as a donor in polysilicon. C. H. Seager in 1979 reported that while a plasma of monatomic hydrogen results in a decrease in resistivity of P doped polysilicon, plasmas of O_2, SF_6 and N_2 can substantially increase the resistivity [48]. Goro Sasaki shows that nitrogen incorporated in chemically vapor deposited (CVD) amorphous silicon results in an increase in the resistivity [49].

This author is aware of only one paper that shows the decrease in resistivity in polysilicon as a result of nitrogen doping, by H Hayashi et al [18]. In this paper, LP-CVD films of polysilicon 0.2 μm thick were implanted with N_2 at 80 keV with doses in the range 1E14 to 1E17 cm^{-2}. These samples were annealed in N_2 at $800^\circ C$ to $1000^\circ C$. A phosphorus doped polysilicon film was deposited at $650^\circ C$ and selectively etched for contacts, and the resistivity was measured at 10 V.

The resistivity was constant for N concentrations less than $1E20/cm^3$ and is equal to non-implanted films (see Fig. 2.9), but at higher

RESISTIVITY vs N CONCENTRATION
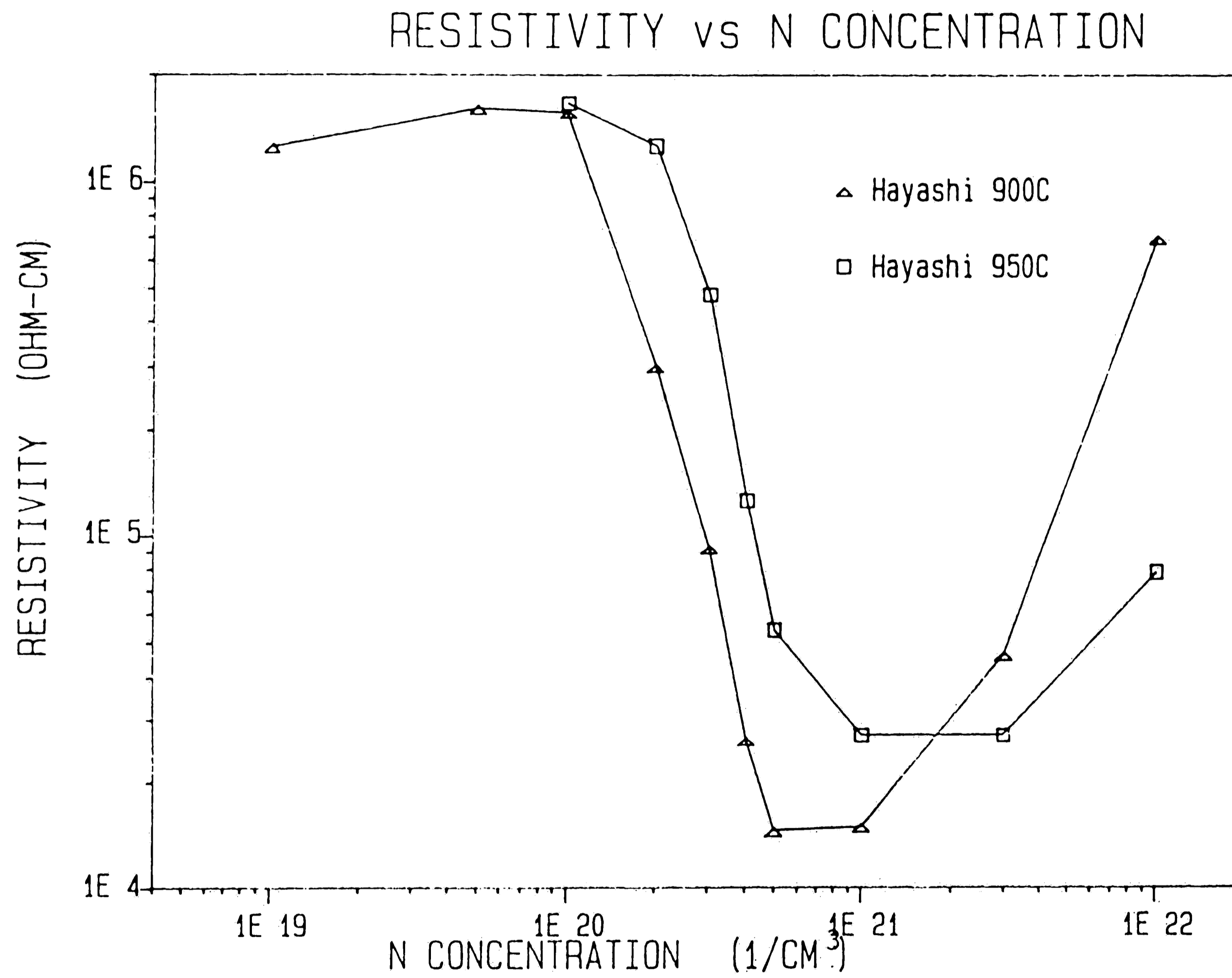
Fig. 2.9   Resistivity vs nitrogen concentration, from ref. 18.

Solid Solubility and Diffusion Coefficients in Crystalline Si

Element	N	C	O	As	B	P
Approx. max. Solid Solubility (atoms/cc)	4.5E15	3.2E17	2.8E18	2E21	6E20	1E21
ref.	[47]	[47]	[47]	[54]	[54]	[54]
D_0 (cm^2/s)	0.87	1.9	0.07	12	0.76	3.85
E (eV)	3.29	3.1	2.44	4.05	3.46	3.66
ref.	[17]	[55]	[55]	[55]	[55]	[55]

Table 2.1   Solid Solubility and Diffusion Coefficients in Crystalline Si.

concentrations, the resistivity drops only 2 orders of magnitude (1.6E6 Ohm-cm to 1.5E4 Ohm-cm for the $900^{o}C$ anneal) and reaches a minimum at about $5E20/cm^{3}$. At higher doses the resistivity increases. The resistivity increase at this point is speculated by Hayashi as being caused by an decrease in the mobility. The resistance of the sample annealed at $900^{o}C$ is lower than that of the $950^{o}C$ sample around the minimum.

The sheet resistance increases as the $900^{o}C$ anneal time is increased (see Fig. 2.10), but at a low temperature ($400^{o}C$) anneal in hydrogen, the resistivity remains almost constant. This is not unusual since at these low temperatures, hydrogen anneal has no affect on normally doped polysilicon [50] although a plasma anneal with hydrogen causes a reduction in the resistivity by reducing the trapping states [48,50].

H. Hayashi calculates that for a deep donor energy level, the resistivity dependence on doping concentration is much weaker than for a shallow donor, and he assumes that nitrogen is such a deep donor based on a publication by K. L. Brower mentioned earlier [41]. Unfortunately, this measurement of a deep level for nitrogen by Brower was later recanted [43].

ANNEAL TEMPERATURE: $900^{\circ}C$
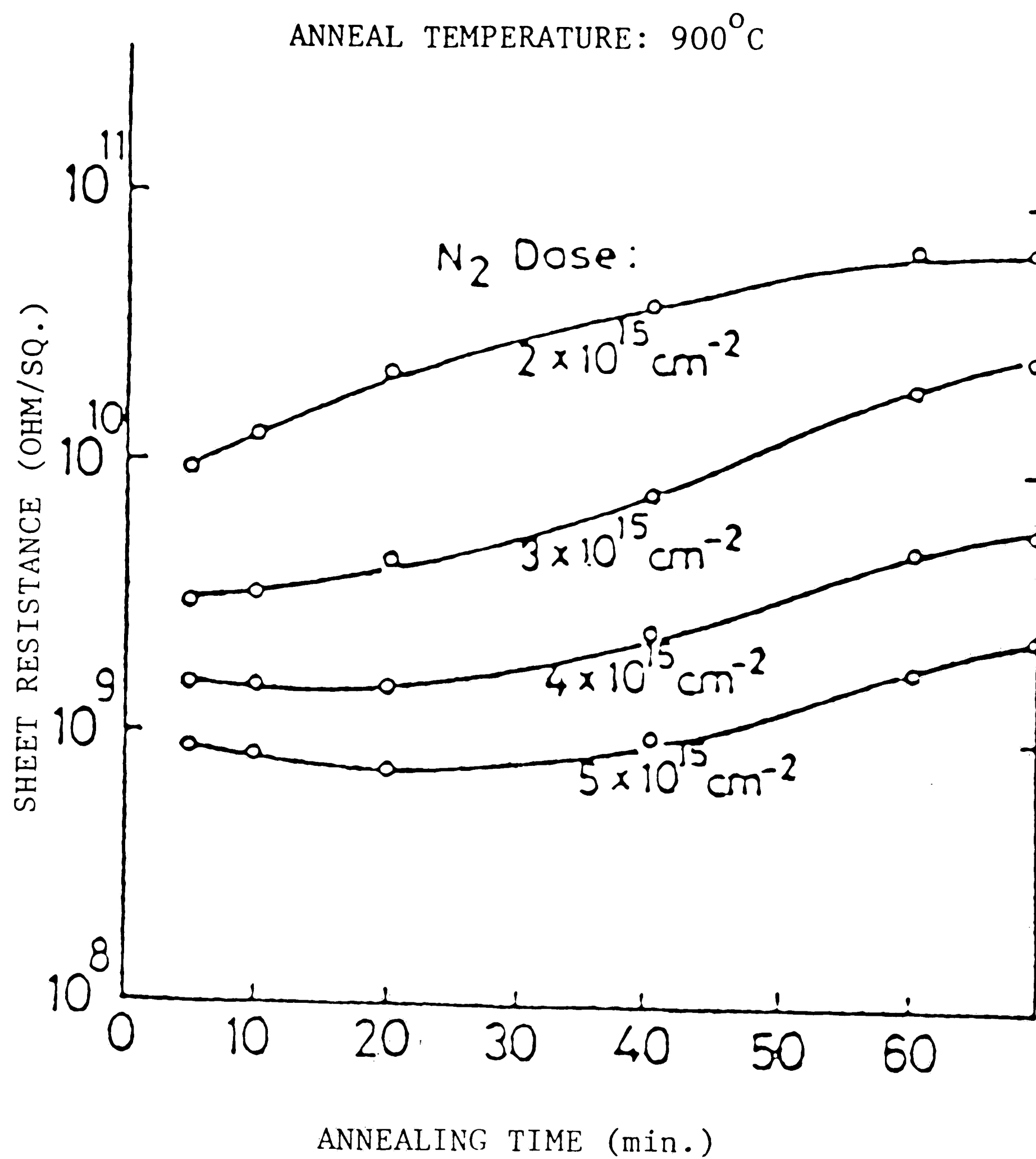
Fig. 2.10 Sheet resistance vs anneal time,
for various N concentrations, from ref. 18.

CHAPTER III

EXPERIMENTAL

A. Resistor Structure

The polysilicon resistor test structure is shown in Fig. 3.1. It consists of sets of 10 parallel resistors, each 3.9 μm wide, 0.51 μm thick and of various lengths from 3.9 μm to 22.9 μm in 1 μm steps. The resistors are connected to polysilicon contact pads by lengths of polysilicon runners, both of which are implanted with 1.0E16 cm^{-2} As at 30 keV. The previously N doped polysilicon resistors are protected from this As implant by the Si_3N_4 capping layer as shown in the cross section in Fig. 3.2. This test structure is part of a test pattern of which there are 5 on a 100 mm wafer, one in the center and 4 which are 15 mm from the edge of the wafer in each quadrant.

B. Resistor Processing

The processing of these wafers was done at AT&T Technologies, Inc. Allentown Works in Pennsylvania. The polysilicon was deposited on 10,000 Å of SiO_2 on p-type (100) silicon substrates. Polysilicon was deposited by low pressure chemical vapor deposition (LPCVD) at 619°C at a pressure of 0.4 Torr. Silane diluted with nitrogen was used for the deposition source, and the deposition rate was about 70 Å per minute. An initial thickness of 5900 Å of polysilicon was deposited. A thin filter oxide of 200 Å is grown at 900°C for 33

33

Contact
Pad

L=12.9 μm

L=11.9 μm

As + N doped
Polysilicon
Contact
Pad

Si$_3$N$_4$ Resistor Mask

N doped
polysilicon
resistor
L=22.9 μm

L=21.9 μm
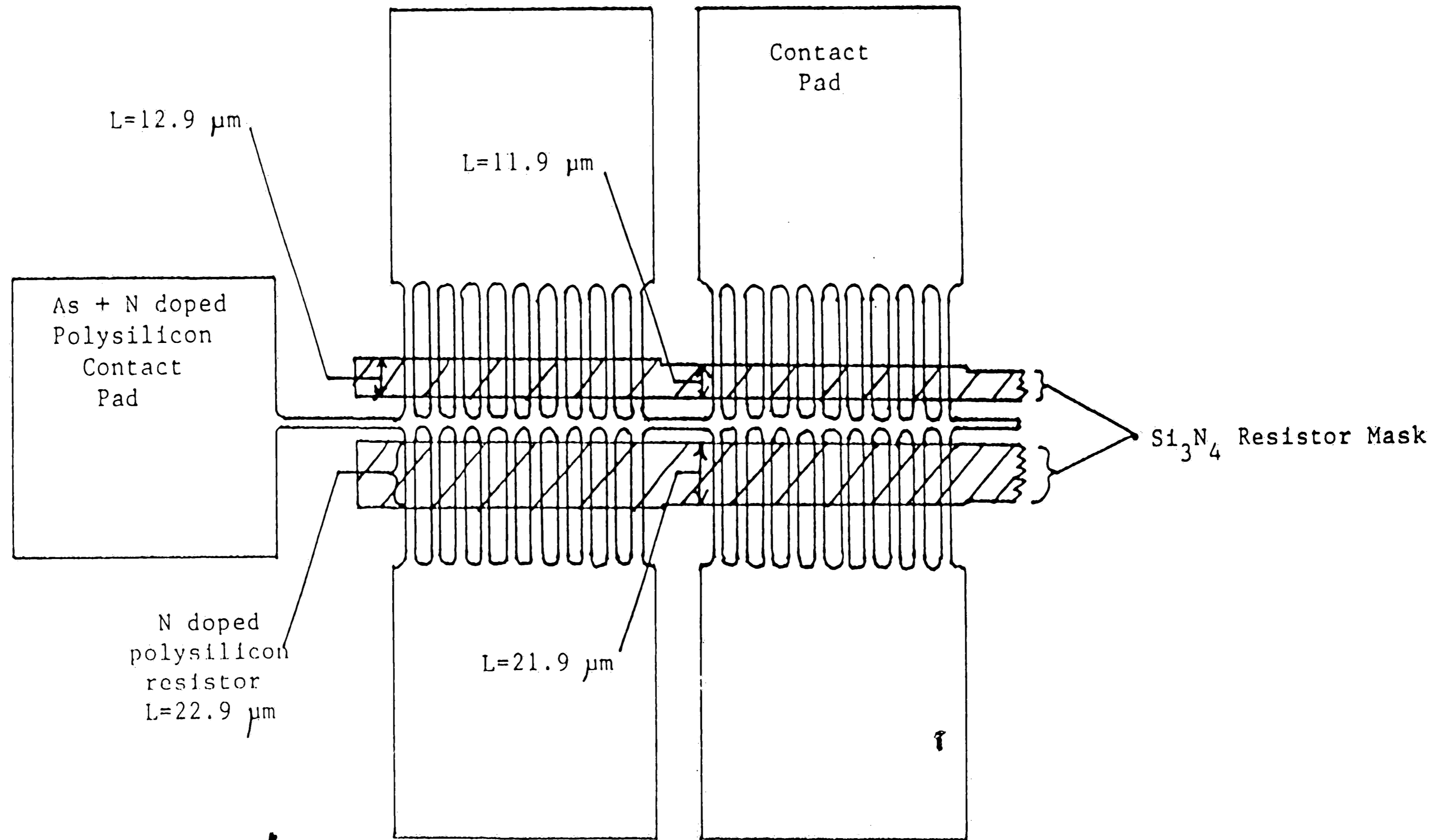
Fig. 3.1   Resistor test structure.
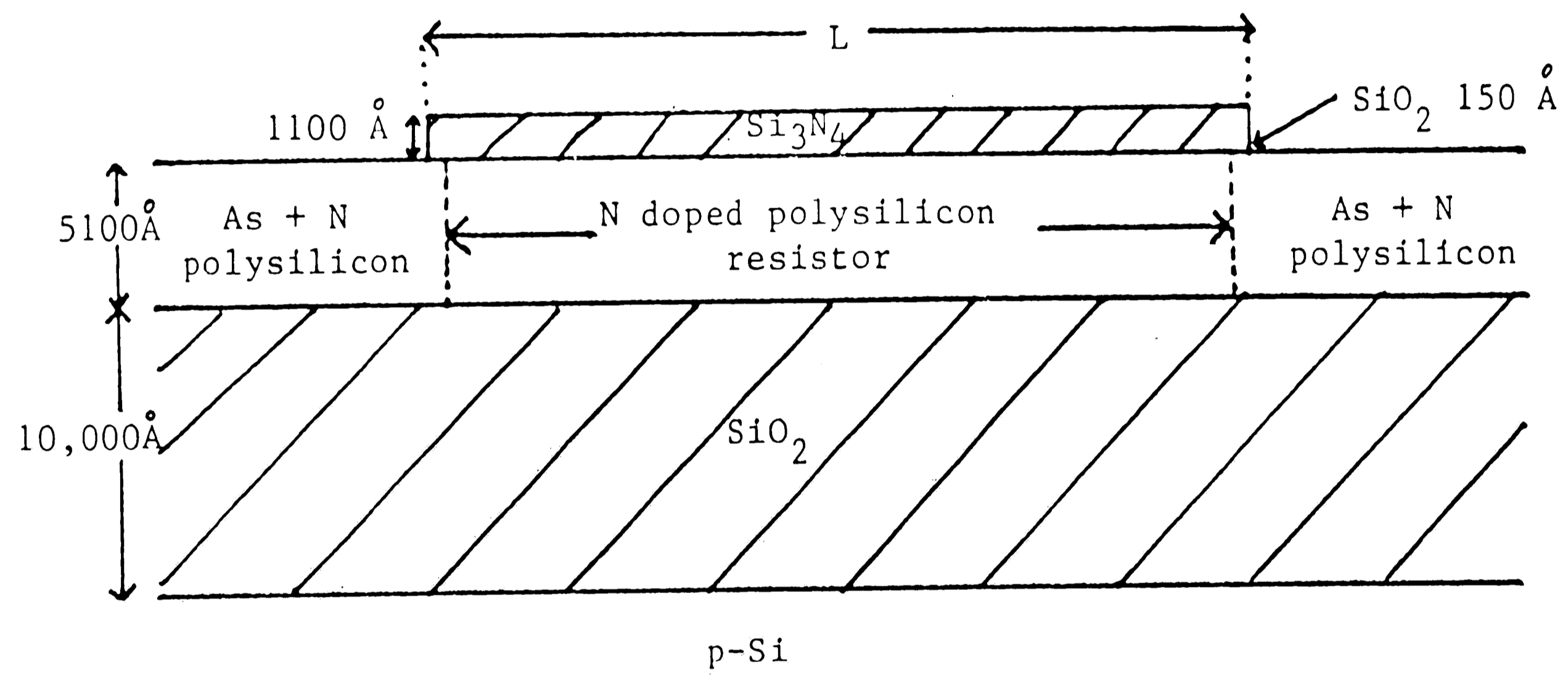
Fig. 3.2 Resistor test structure, cross section.

min and the polysilicon is implanted with N_2 at 160 keV. The beam current was about 4.5 mA and the implants were done in doses of a maximum of 2E16 cm^{-2} increments and the wafers were allowed to cool back to room temperature to prevent overheating. The beam power was about 720 watts.

The implant doses were much higher than normally used in semiconductor processing and the implant times were consequently very long. The run time per wafer ranged from 4 min/run for the 3.16E15 cm^{-2} to 12 hours for the dose of 1.2E17 cm^{-2}. The long times involved prohibited going to a higher dose implant in this experiment and limited the number of samples that were implanted.

After the N_2 implant, the polysilicon was oxidized in steam at 950^OC for 10 min, growing 1700 Å of a masking oxide, and photoresist was applied and patterned. The oxide was etched with buffered HF acid and the polysilicon was then etched in a plasma of Freon 14 (CF_4) and O_2. The photoresist and the masking oxide were removed, and a thin layer (about 150 Å) of oxide was grown at 950^OC for 22 min which acts as a pad oxide for the following layer of Si_3N_4, which is deposited to a thickness of 1100 Å by LPCVD and patterned by a plasma etch. Arsenic is then implanted at 30keV at a dose of 1E16 cm^{-2} and annealed in nitrogen at 900^OC for 60 min. The nitride layer acts as an implant mask for the resistor, and the As implant creates highly conductive runners and allows for an ohmic contact

with metal probes.

After processing as above, resistance measurements can be made, and the wafers can then be treated at higher temperatures and remeasured. The reason that aluminum contacts were not put down was to allow the wafers to be further heat treated.

Some wafers were treated at higher temperatures in order to simulate the affects of subsequent processing in a normal manufacturing process. Two wafers were treated at $1000^\circ C$ in O_2 for 30 min, and these two wafers and two others were treated at $1100^\circ C$ for 30 min in N_2.

C. Measurements

Resistance and I-V measurements were made using an HP 4140B picoammeter/DC voltage source, controlled by an HP 9836 microcomputer, and the wafers were placed on a chuck which could be heated in order to measure temperature affects. The wafers and the chuck were placed in a light-tight, shielded box. The probe contact resistance and its linearity were checked and measured by placing both probes close to each other on a single contact pad. The total resistance was 400 ohms for two probes and the I-V curve was linear.

The variables in this experiment are: applied voltage (V), measured

current (I) which gives the resistance (R) for each V, nitrogen concentration, resistor length (L), and temperature (T). The measurements that were made in order to fully characterize the resistors were: R at 5 V at each concentration for L = 13.9 μm, I-V curves for various L's at 23°C, I-V curves at various temperatures for L = 13.9 μm, R vs. L at 5 V, and the affect of subsequent heat treatments on some of the above results. The reason 5 V was used in some of the measurements was that this is a typical voltage drop across a resistor if it is used as a load element in an inverter or memory cell.

CHAPTER IV

RESULTS AND DISCUSSION

A. Resistance vs. Concentration

The resistance of the 13.9 μm long resistors on all of the test patterns was measured at 5 V at 23°C. A graph of the resistivities for each N concentration is presented in Fig. 4.1. The bars are one sigma limits. A table of these data is listed in Table 4.1. There were 15 resistors (3 wafers) measured for each concentration, except for the highest ($4.71E21/cm^3$) and the unimplanted samples, where only 10 measurements each (2 wafers) were taken. This length of resistor chosen represents a typical length that may be used in a static RAM memory cell, which is a compromise between a shorter resistor with a more severe non-linear affect (to be discussed in the next section) and a longer resistor that consumes too much area. Five volts was chosen since it represents the typical case of an output of 0 in a basic inverter.

Fig. 4.1 shows that the effect of the N implant is not felt until the concentration is above about $3E20/cm^3$, and that the resistance is lowered by only a factor of 30 over the range of concentrations, and increases at the highest concentration of $4.7E21/cm^3$. This is in contrast to the case of As implanted into polysilicon, where the

39
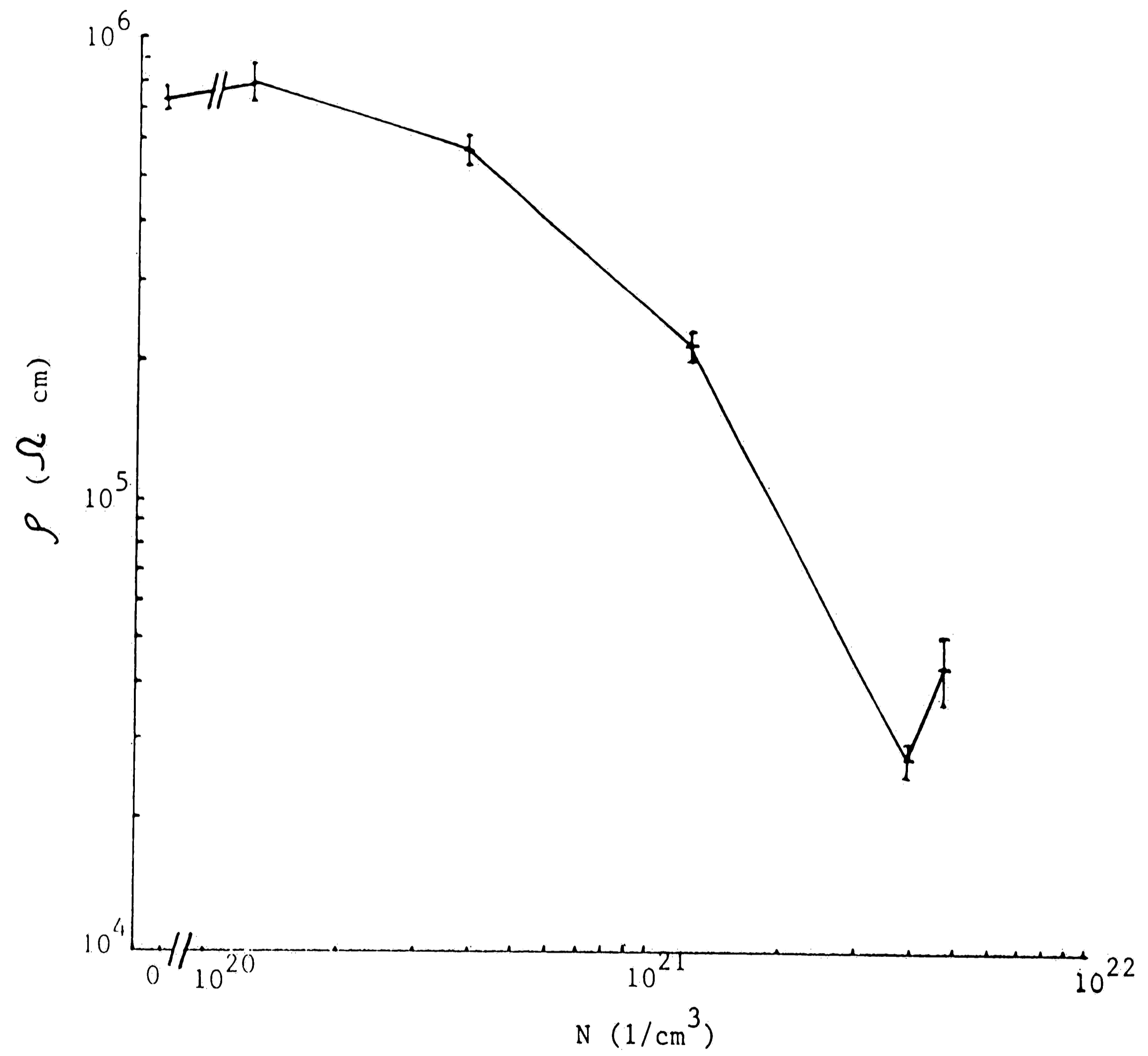
Fig. 4.1 Resistivity vs nitrogen concentration, this work.

RESISTANCE VS IMPLANT DOSE

Conditions: 13.9 μm resistor length
             5 V applied
             temperature = 23°C

Dose	Concentration	Resistance	Resistivity	#
$1/cm^2$	$1/cm^3$	Ohm	Ohm-cm	meas.
0	0	5.12 ± 0.32 E9	7.33 ± 0.46 E5	10
3.16 E15	1.24 E20	5.54 ± 0.52 E9	7.93 ± 0.74 E5	15
1.00 E16	3.92 E20	3.97 ± 0.29 E9	5.68 ± 0.42 E5	15
3.16 E16	1.24 E21	1.50 ± 0.11 E9	2.15 ± 0.16 E5	15
1.00 E17	3.92 E21	1.90 ± 0.17 E8	2.72 ± 0.24 E4	15
1.20 E17	4.71 E21	3.03 ± 0.51 E8	4.34 ± 0.73 E4	10

Table 4.1   Resistance vs implant dose.

Fig. 4.2 Resistivity vs nitrogen concentration, this work compared with Hayashi, ref. 18.

RESISTANCE VS IMPLANT DOSE

Conditions: 13.9 μm resistor length
5 V applied
temperature = 23°C

Dose $1/cm^2$	Concentration $1/cm^3$	Resistance Ohm	Resistivity Ohm-cm	# meas.
0	0	5.12 ± 0.32 E9	7.33 ± 0.46 E5	10
3.16 E15	1.24 E20	5.54 ± 0.52 E9	7.93 ± 0.74 E5	15
1.00 E16	3.92 E20	3.97 ± 0.29 E9	5.68 ± 0.42 E5	15
3.16 E16	1.24 E21	1.50 ± 0.11 E9	2.15 ± 0.16 E5	15
1.00 E17	3.92 E21	1.90 ± 0.17 E8	2.72 ± 0.24 E4	15
1.20 E17	4.71 E21	3.03 ± 0.51 E8	4.34 ± 0.73 E4	10

Table 4.1   Resistance vs implant dose.

Fig. 4.2 Resistivity vs nitrogen concentration, this work compared with Hayashi, ref. 18.

resistance may drop 5 orders of magnitude over only a 2 decade change in the As concentration [1-8,10-14,16], see Fig. 2.3. As mentioned chapter 2, there are similar curves for B and P dopants.

In Chapter 2, equations 17 and 18 show the conductivity is approximately proportional to the grain size, L. It will be shown in the next section that the grain size as calculated from the I-V measurements vary only by a factor of about 2.5 from the undoped polysilicon to heavily doped polysilicon. This grain size variation therefore contributes to the lowering of the resistivity with an increase in the N concentration, but only accounts for about 10% of this effect.

A comparison of these data can be made to the data from Hayashi, mentioned in Chapter 2, Fig. 2.9, ref. [18]. These data have been converted to the same dimensions as used in this work and plotted on the same graph, see Fig. 4.2. This graph shows that both sets of data have similar characteristics. There is about a factor of 100 decrease in resistivity in the data from Hayashi, whereas in the present data the ratio is about 30. Both of these factors are much less than what is seen for normal dopants. The decrease in resistivity takes place around $2E20/cm^3$ and increases again around $3E21/cm^3$. It should be noted that for both of these experiments, the N concentration in Si exceeds the measured solid solubility in

single crystal Si of $4.5 \times 10^{15} \text{cm}^{-3}$ [17,47].

As mentioned in Chapter 2, Hayashi attributes the increase in resistivity at the higher doses to a decrease in the mobility. This decrease could be caused by increased impurity scattering caused by the formation of electrically active complexes of $Si_x N_x$, although one would think that increased annealing temperatures would accelerate this formation.

Another explanation for the increase in the resistivity at the higher concentrations is a reduction in the number of donors. Only a small fraction of N atoms are electrically active and has a concentration dependence in single crystal Si which peaks at 0.6% for 10^{17}cm^{-3}. The concentration reduction at higher doses may be caused by the formation of N_2 or $Si_3 N_4$ [17,44,45].

B. I-V Characteristics

I-V measurements were made on 3.9 μm, 8.9 μm, 13.9 μm and 18.9 μm resistors at room temperature for each N concentration. The voltage range was 0 - 30 V. This range was higher than 5 V in order to highlight the nonlinear effects. Sample I-V curves can be seen in Figs. 4.3 - 4.6, for doses 1E16 and $1E17/\text{cm}^2$. It can be seen from these curves that the I-V characteristics are not linear for the smaller resistor lengths and for the lower concentrations. The
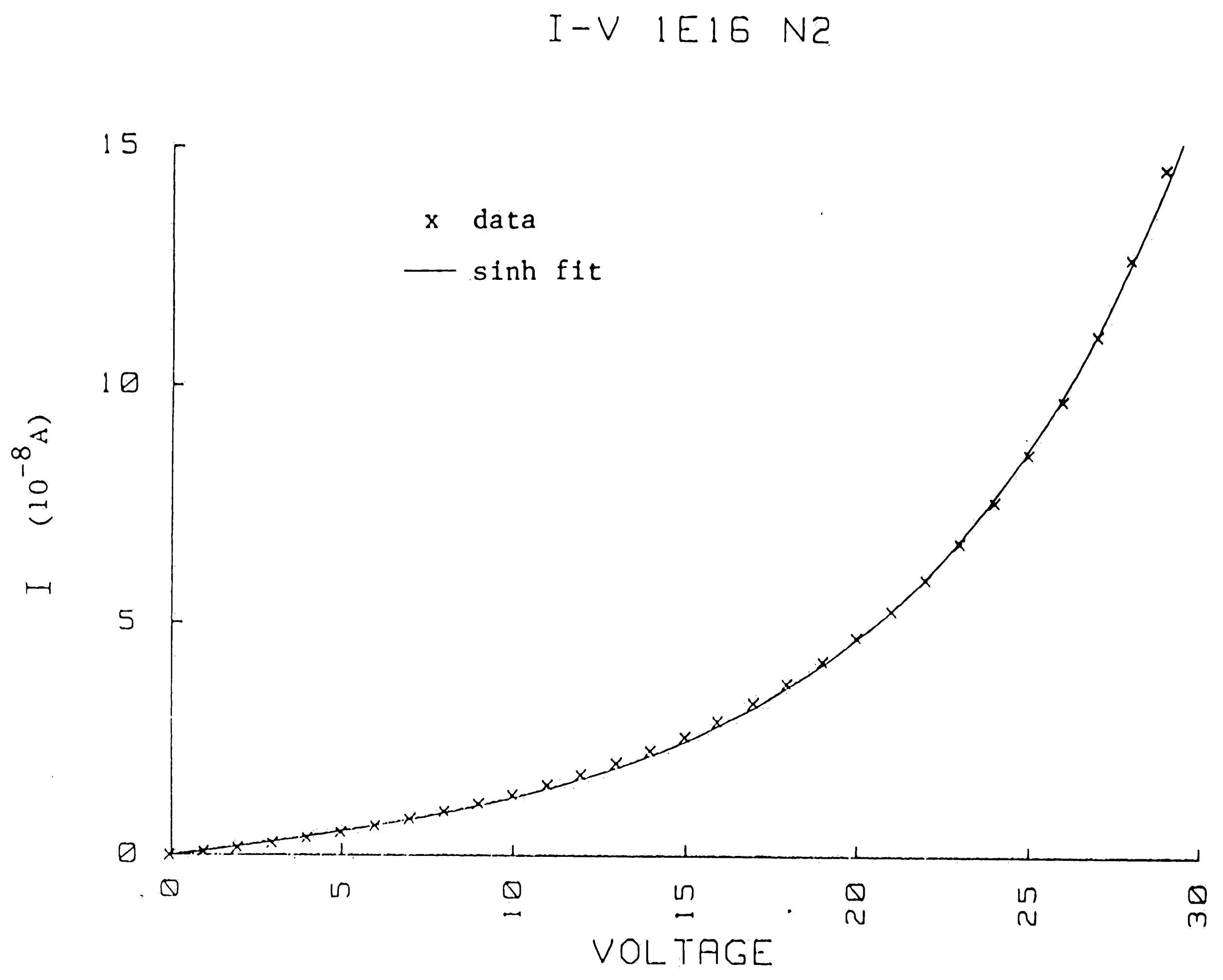
Fig. 4.3 I-V curve, 3.9μm resistor, 1E16 implant dose.
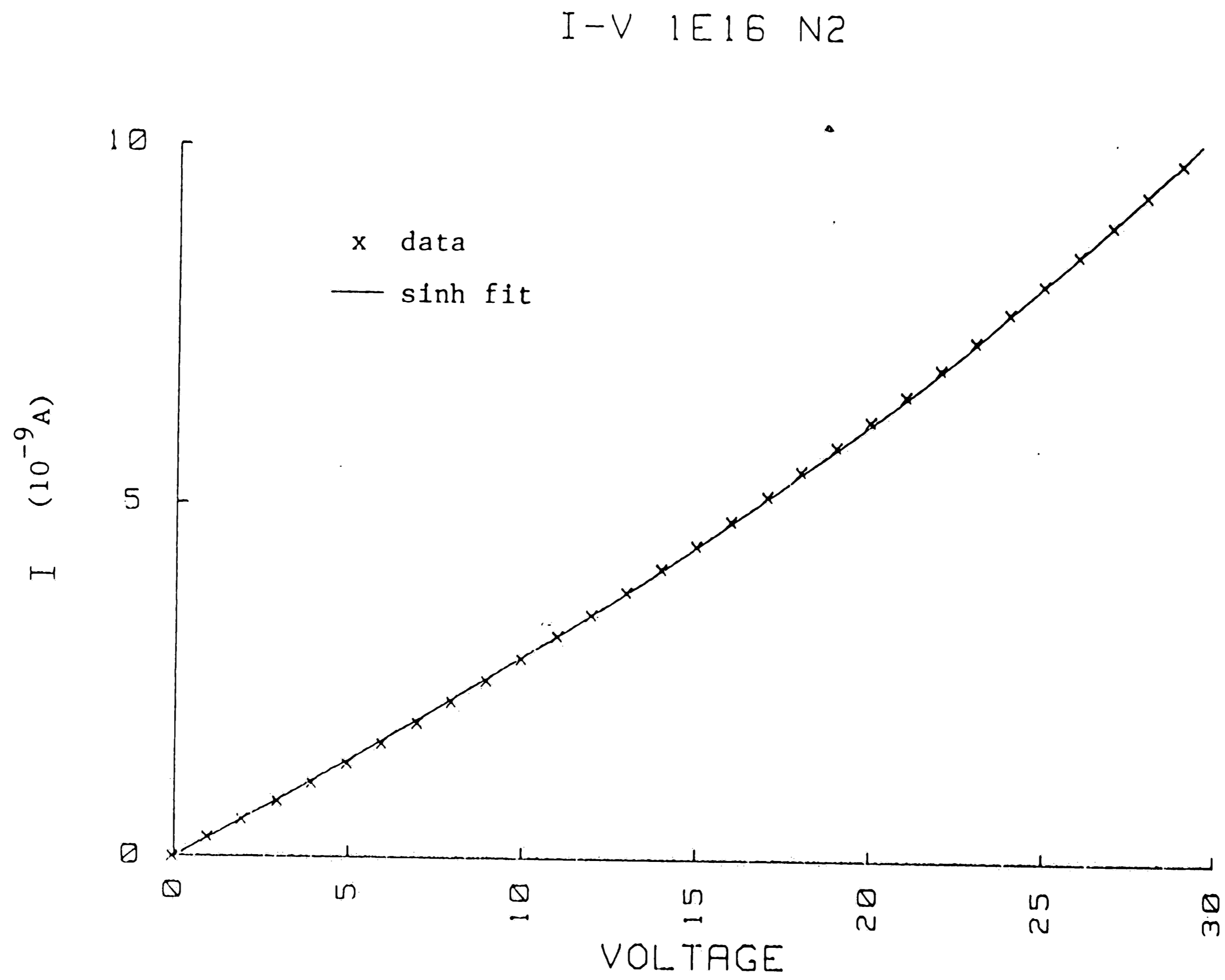
I-V 1E16 N2

Fig. 4.4 I-V curve, 13.9μm resistor, 1E16 implant dose.
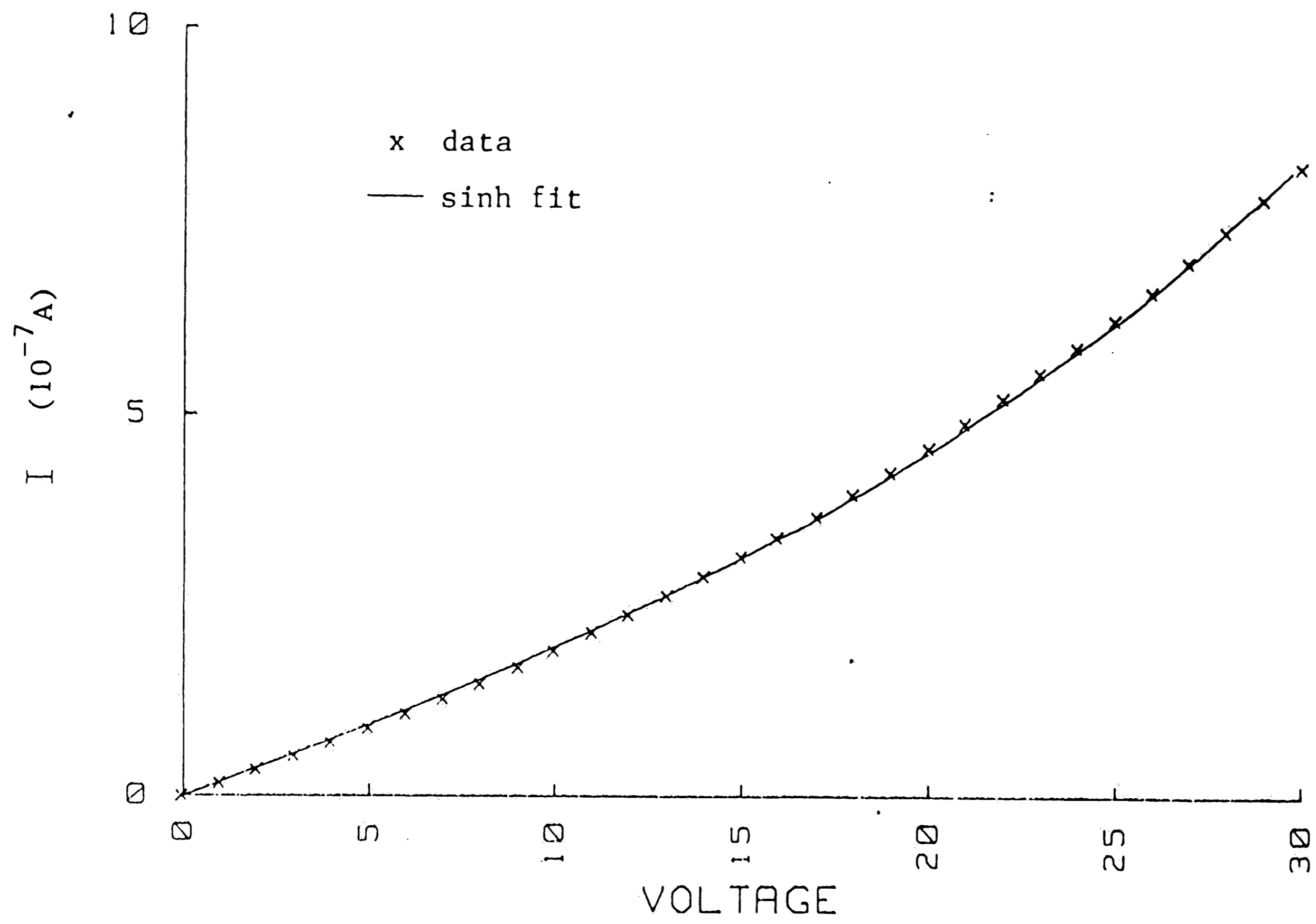
I-V 1E17 N2

Fig. 4.5   I-V curve, 3.9µm resistor, 1E17 implant dose.

I-V 1E17 N2
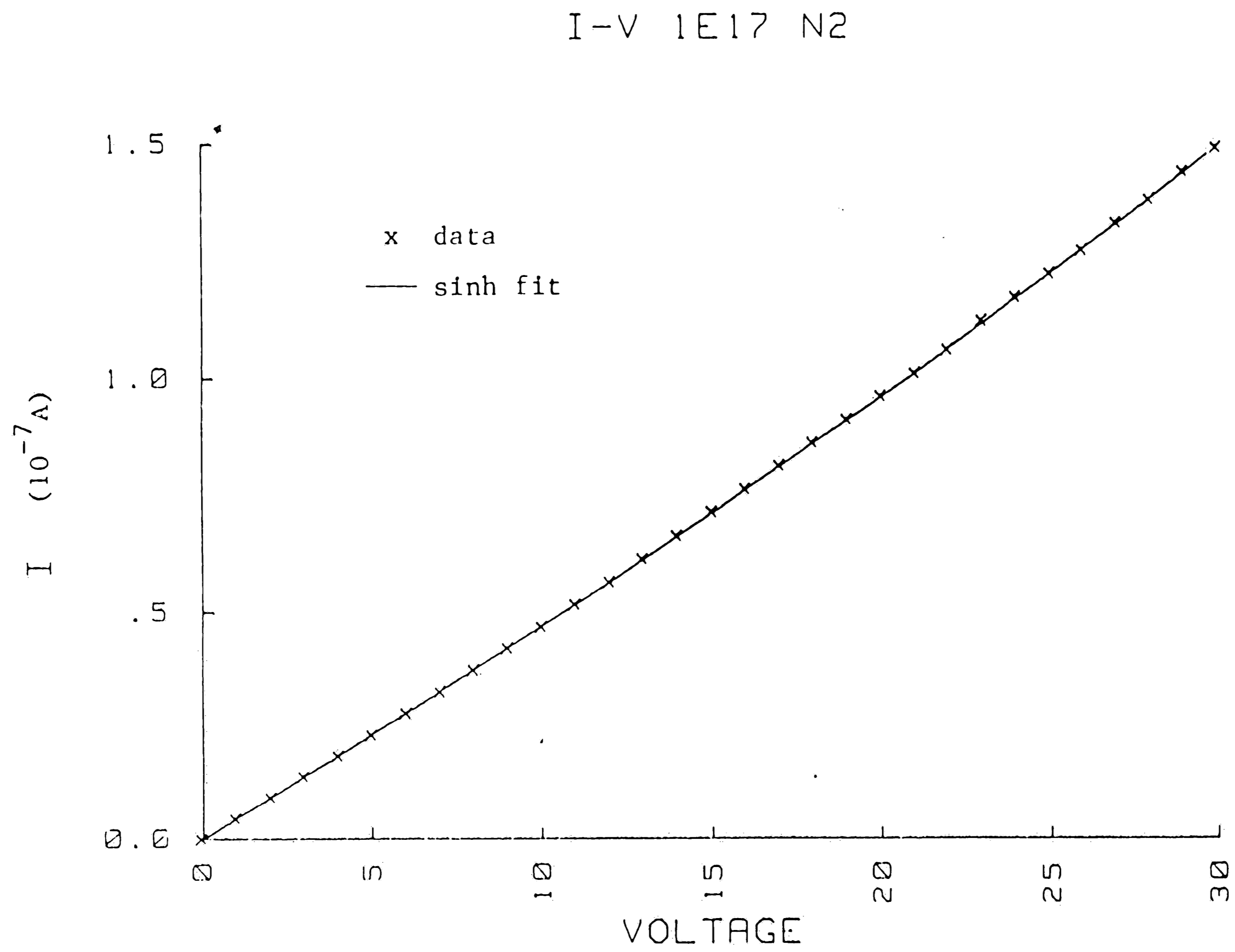
Fig. 4.6   I-V curve, 13.9μm resistor, 1E17 implant dose.

solid lines in these figures are least squares fits to a hyperbolic sine equation: I = Asinh(BV), where A and B are the fitting parameters. A table of the results of these fits is shown in Table 4.2. Note that for some doses, more than one wafer was measured to allow one wafer to be further heat treated while the other is not. The higher the value of B in these fits, the more nonlinear the I-V curve is. The values followed by a "*" are for cases where the sinh fit was not a good fit.

The thermionic emission theory discussed in chapter II predicts that the value of B in the sinh fit of the I-V measurements should be inversely proportional to the resistor length (see eqn. 25).

$$B = l_g q/2LkT$$

where l_g is the average polysilicon grain size, and L is the resistor length. Using kT/q = 0.0259 eV, and the measured values of L, the grain size as derived from the fitting parameter B can be calculated and is shown in the lower portion of Table 4.2. It can be seen from this table that the values of l_g are fairly consistent for all but the concentrations $1.2E20/cm^3$ and the unimplanted samples, where the doping levels are too low to allow thermionic emission.

At low doping levels, the required condition for thermionic emission, that the barrier height be larger than kT, is violated. From equation (4) in Chapter 2,

$$V_B = qL^2N/8\epsilon$$

IV CURVE FIT PARAMETERS
VARIOUS LENGTHS
I=Asinh(BV)

B VALUES
L=RESISTOR LENGTH (μm)

N2 DOSE	WAFER	L=	3.9	8.9		13.9		18.9	
0	31		0.2391	0.0613	*	0.0510	*	0.0472	
3.2E+15	25		0.1943	0.0615	*	0.0496	*	0.0437	*
1.0E+16	32		0.1230	0.0489		0.0370		0.0326	
1.0E+16	23		0.2893	0.0476		0.0332		0.0277	
3.2E+16	46		0.0989	0.0422		0.0289		0.0244	
1.0E+17	49		0.0507	0.0289		0.0210		0.0157	
1.0E+17	48		0.0491	0.0289		0.0192		0.0149	
1.0E+17 ##	48		0.0692	0.0314		0.0218		0.0166	
1.2E+17	1		0.0547	0.0344		0.0281		0.0177	

CALCULATED GRAIN SIZE – ANGSTROMS

N2 DOSE	WAFER	3.9	8.9		13.9		18.9		AVG.
0	31	483	283	*	367	*	462		399
3.2E+15	25	393	284	*	357	*	428	*	365
1.0E+16	32	248	225		266		319		265
1.0E+16	23	584	219		239		271		329
3.2E+16	46	200	195		208		239		210
1.0E+17	49	102	133		151		154		135
1.0E+17	48	99	133		138		146		129
1.0E+17 ##	48	140	145		157		162		151
1.2E+17	1	111	159		202		173		161

* => POOR CURVE FIT
=> POST 1000C ANNEAL

Table 4.2   I-V curve fit parameters - various lengths.

For $1.2E20/cm^3$, assuming only 0.1% of the dopants are ionized and
that the grain size L = 200 Å, we have

V_B = 0.009 V < kT/q = 0.026 V for 300°K.

There is a slight trend for the calculated grain size to increase
for the increasing resistor length, which is unexplained by the
simple thermionic emission theory. This effect may be caused by the
influence of the As junctions on either end of the resistors, which
have a greater effect on the shorter resistors. Another possibility
is the statistical fluctuations of grain sizes and barrier heights
over an individual sample [9]. The simple theory is based on a
single grain size and barrier height.

The calculated grain sizes show a decrease with an increase in the N
concentration. This is not caused by increased heating due to the
increased implant doses because higher temperatures cause an in-
crease in grain sizes [16,25,30,51]. The effect of doping levels of
normal n-type dopants is an increase in the grain sizes with an
increase in doping levels [11,31,32,34,35] and therefore does not
explain the observations. A possible mechanism for the reduction in
grain size with the increase in the N concentration is the formation
of Si_3N_4 at the grain boundaries which inhibits grain growth. This
mechanism has been suggested to explain the fact that the grain
sizes for CVD oxygen doped polysilicon also decrease with increasing
oxygen concentrations, possibly forming SiO_2 at the intergrain

boundaries which prevents grain growth during annealing [24].

It has been observed by other authors that the calculated grain size varies with the doping concentration of normal dopants and with the measurement temperatures [9]. The variation with doping concentration or temperature was shown in [9] not to be caused by the actual grain size as shown in TEM measurements, but is most likely due to the large variation in grain sizes within a sample. This causes various conduction paths to be preferred depending on which grains are completely depleted or not, which in turn are dopant and temperature dependent.

C. Resistance vs. Length

Room temperature measurements of resistance vs. length for L = 3.9 – 22.9 μm in 1 μm steps were made at 5 V for each implant dose. The results are shown in Fig. 4.7 for the 3 lowest doses, and in Fig. 4.8 for the 3 highest doses. It can be seen that the relationship is reasonably linear, especially for the higher doses. For 0 N_2 and 3E15 N_2, the zero resistance intercept is very negative. For the other doses it is reasonably close to zero.

John E. Mahan et. al. [29] have shown that for undoped polysilicon with heavily As doped n^+ polysilicon contacts at either end of the nominally intrinsic polysilicon resistor, similar to the structure

52
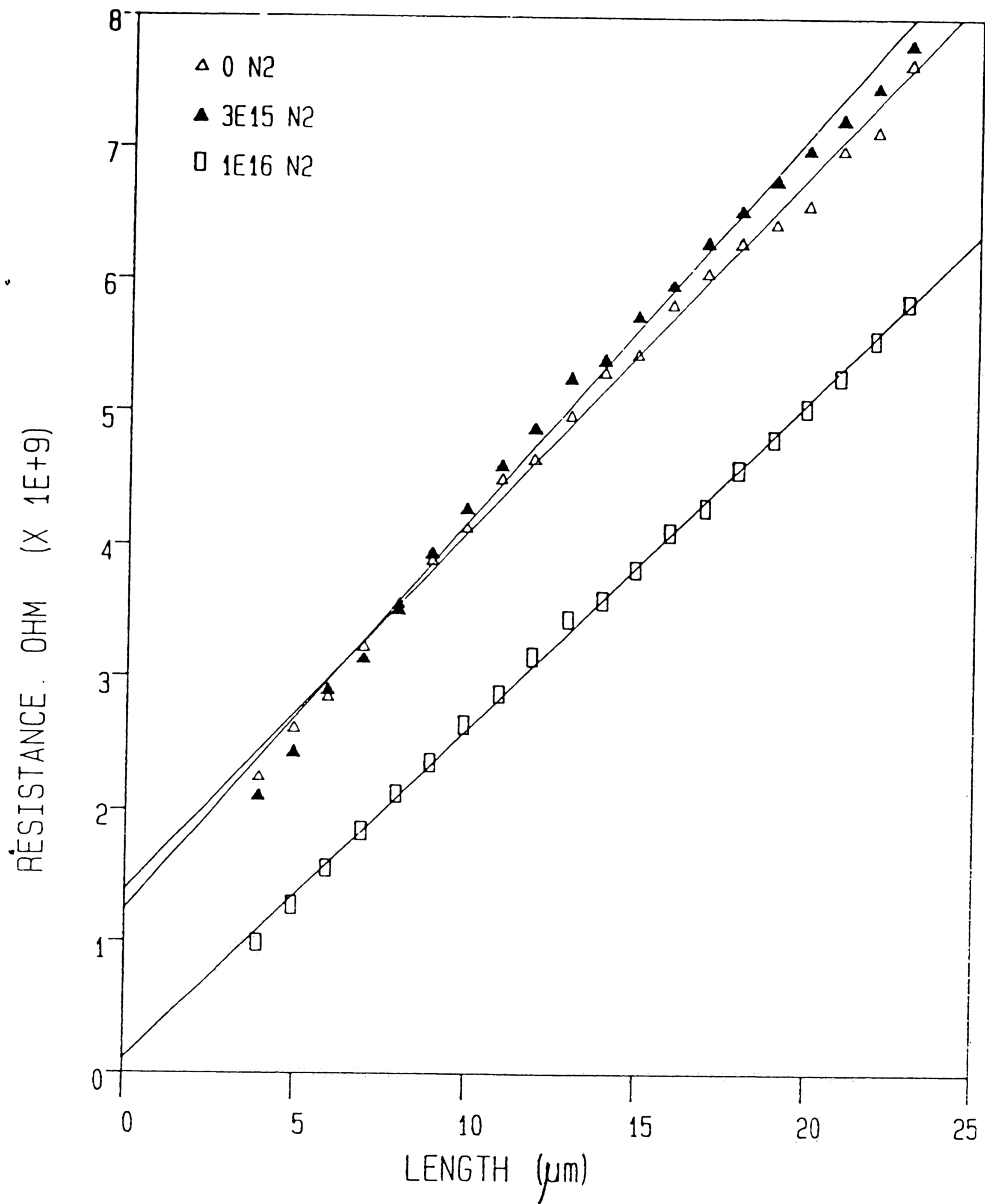
Fig. 4.7   Resistance vs length, lower N concentrations.

53
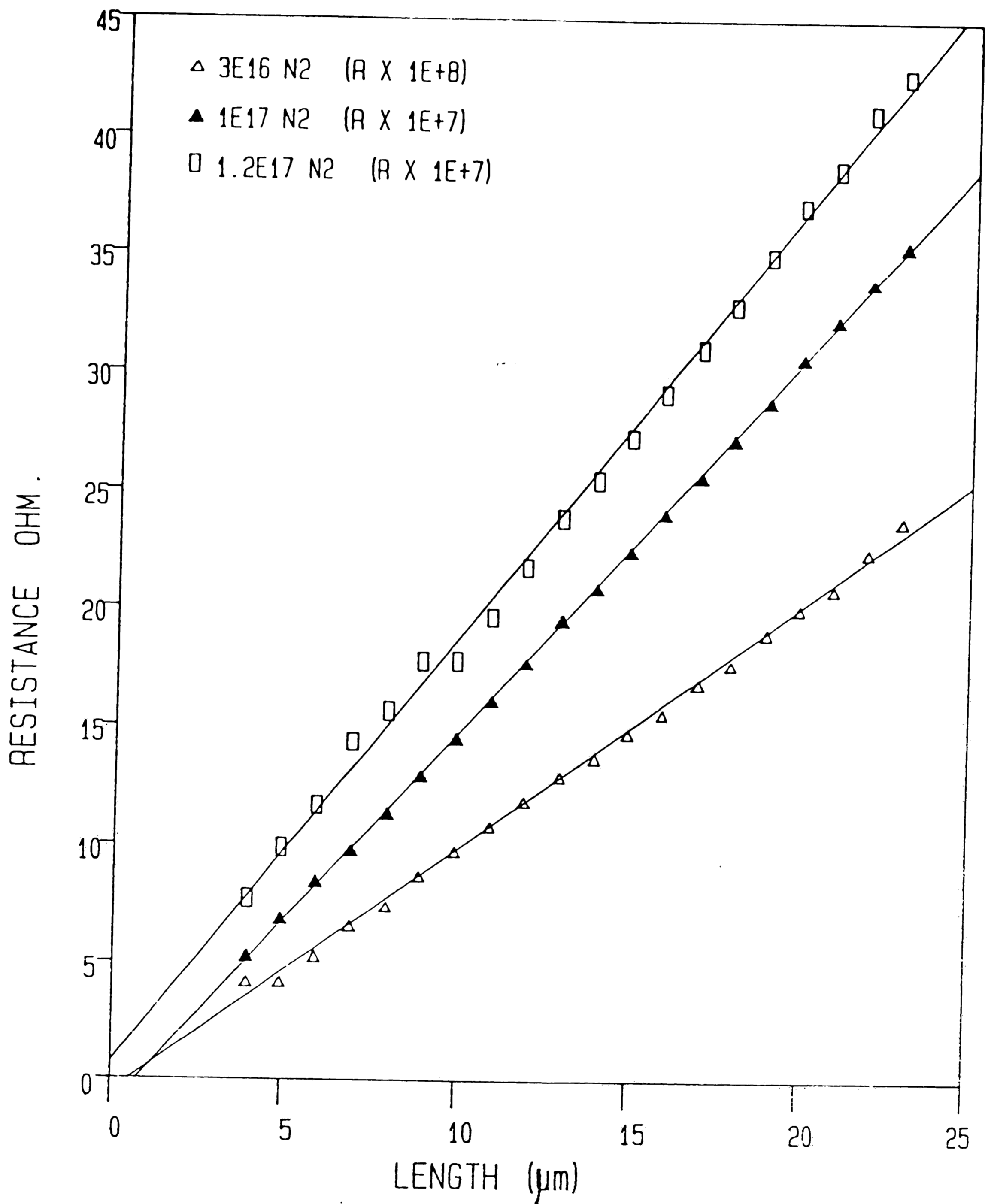
Fig. 4.8 Resistance vs length, higher N concentrations.

54

in this study, there is a nonlinear resistance vs length characteristic due to the n^+-i junctions at either end of the resistor which is the major contributor to the resistance. The measured resistance versus length is similar to the two lowest doped samples in this study and Mahan attributes this nonlinear characteristic as being due to the avalanche breakdown of the reverse biased n^+-i diode on one end of the resistor, with the current being limited by the intrinsic polysilicon resistor. The low breakdown voltage is explained by the fact that in polysilicon the junction will not be planar and field enhancement will occur at junctions with small radii creating a low or soft breakdown. This avalanche breakdown will add a fixed component to the resistance, accounting for the non-zero intercept. At higher doping levels the n^+-i junctions are no longer present and a more linear R vs. L characteristic is observed.

The lowering of the resistance at small resistor lengths is attributed to As diffusion into the polysilicon resistor region. The As diffusion is retarded when there is a significant concentration of N in the polysilicon, as is explained later in the discussion of annealing. For the lightly doped or undoped samples, the As diffusion is noticeable in the R vs. L measurements in Fig. 4.7.

The fact that for N doped polysilicon the R vs. L measurements are approximately linear is supported by the I-V characteristics dis-

55

cussed above. For 5 volts applied and for the shortest resistor (3.9 um), the argument of the sinh fit (see Table 4.2) is small enough that it is nearly linear, i.e.

$$I = A*sinh(B*V) \cong A*(B*V) \quad for \ V = 5V.$$

D. I-V Temperature Effects

The I-V characteristics of 13.9 μm long resistors were measured over a temperature range of 25°C to 150°C. Plots of the measured currents for 1V and 5V are shown in Figs. 4.9 and 4.10. The solid lines are least squares fits to the data. The curves for all but the highest implant dose .(1.2E+17) follow the Arrhenius relationship fairly well.

The calculated activation energy from these curve fits are shown in Table 4.3. As before, there was more than one wafer measured for some implant doses. A graph of the activation energy vs. N concentration is shown in Fig. 4.11, for both applied voltages. It can be seen that for low doses the activation energy is about 1/2 the Si bandgap (E_g = 1.12 eV), as expected, and for higher concentrations the activation energy lowers to about 0.36 eV, and increases slightly at the highest concentration.

This change in the activation energy is much more gradual than the case for As implanted polysilicon [2,7,19] where a change in the

56
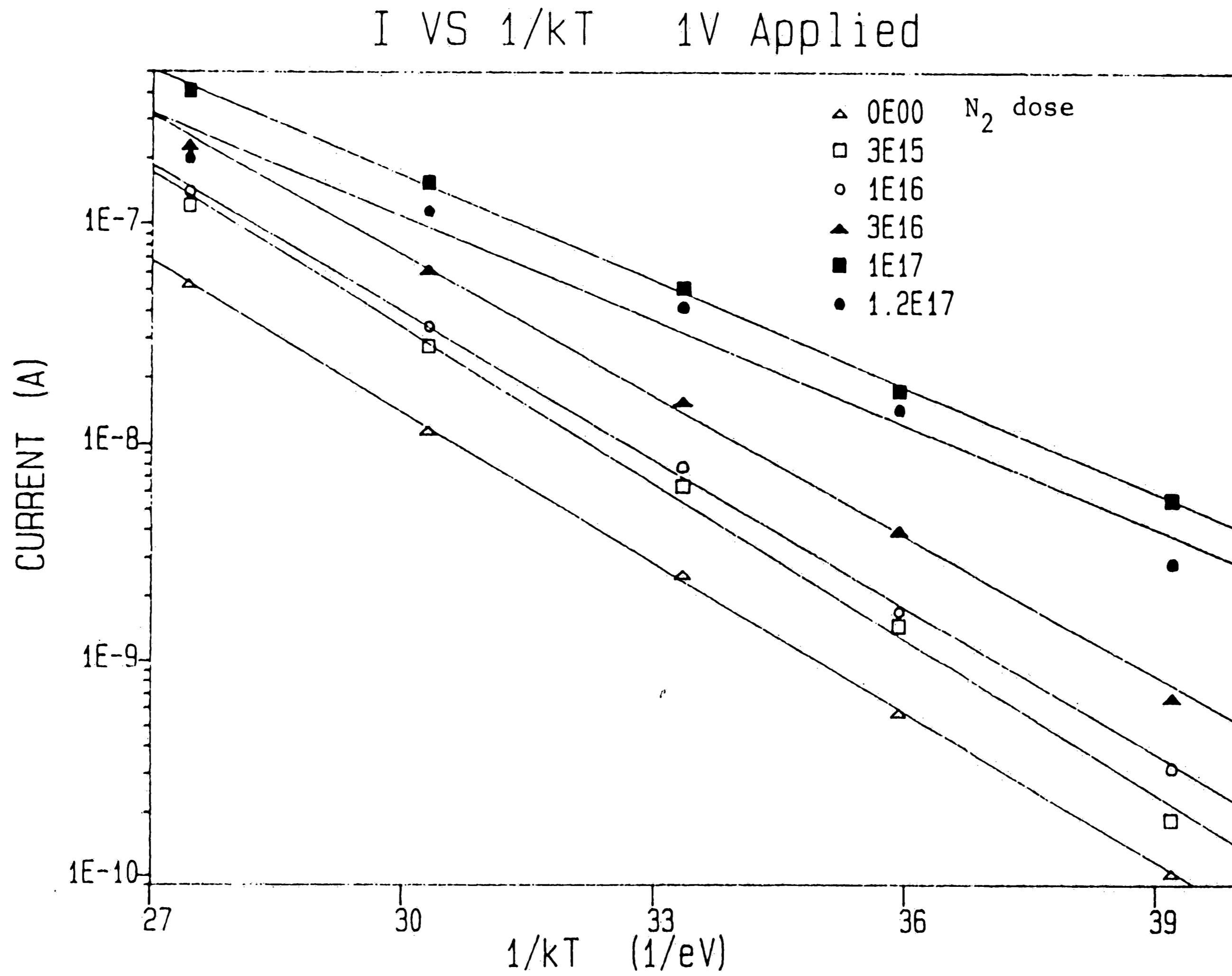
Fig. 4.9 Current vs 1/kT, 1V applied.
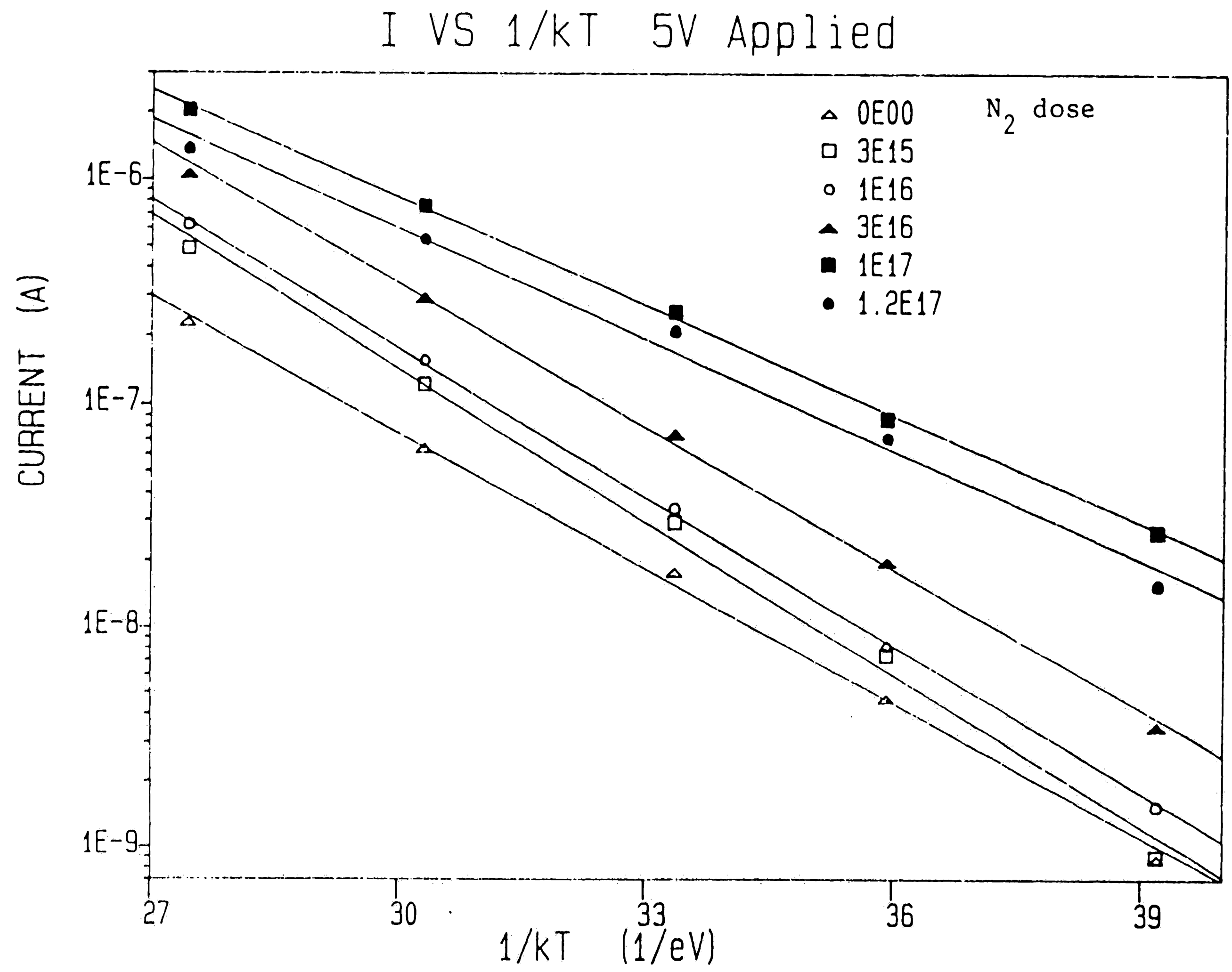
I VS 1/kT 5V Applied

Fig. 4.10 Current vs 1/kT, 5V applied.

ACTIVATION ENERGIES

ACT. ENERGY 1/eV

APPLIED VOLTAGE

N2 DOSE	WAFER	1 V	5 V
0	31	0.5303	0.4674
3.2E+15	25	0.5477	0.5290
1.0E+16	32	0.5324	0.5244
1.0E+16	23	0.5200	0.5111
3.2E+16	46	0.4931	0.4879
1.0E+17	49	0.3720	0.3710
1.0E+17	48	0.3605	0.3607
1.2E+17	1	0.3657	0.3812

Table 4.3 Activation energies vs implant dose.
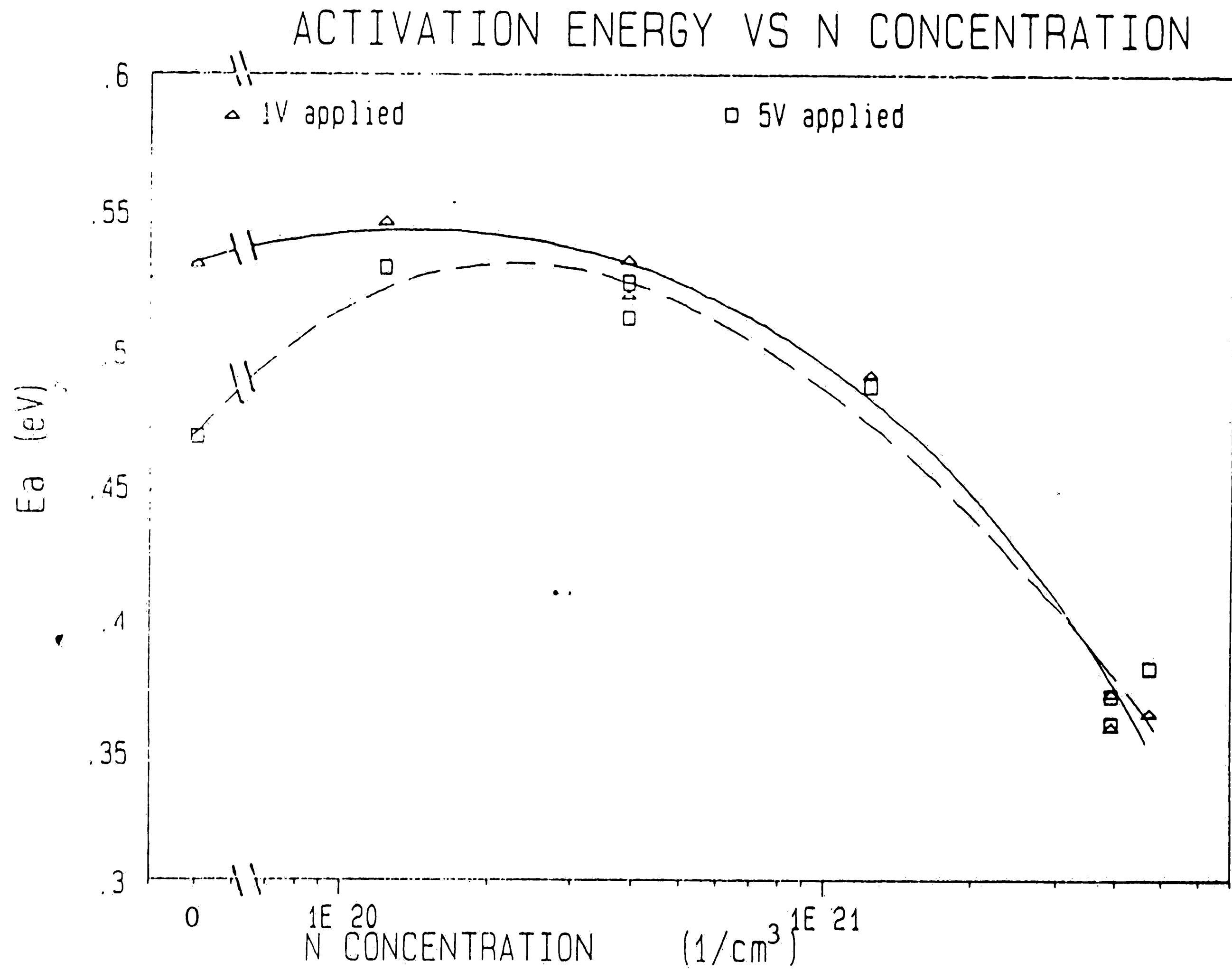
Fig. 4.11 Activation energy vs N concentration, 1V and 5V applied, (lines are aids to the eye).

doping concentration from 1E16/cm^3 to 1E18/cm^3 lowers the activation
energy from 0.51 eV to about 0.06 eV, or for boron doped polysilicon
(see Fig. 2.7).

This more gradual change is more suited to integrated circuit use
because the higher activation energy better matches the activation
energy for the reverse bias junction leakage which is the major
leakage mechanism in static RAM memory cells. For Si, this reverse
bias leakage is due to generation in the space charge region and is
[28]:

$$J_R = q n_i W / \tau_e$$

where W is the depletion layer width, and τ_e is the effective life-
time. The major temperature dependence is due to n_i and is:

$$n_i \propto T^{3/2} \exp(-E_g/2kT)$$

The activation energy for this leakage mechanism is $-E_g/2 = 0.56$ eV.

The I-V curves at the various temperatures were fit to the hyper-
bolic sine relationship to test the validity of the thermionic
emission theory. The curves obeyed the sinh relationship over all
of the temperature range except for the highest temperature (150°C),
and for the two lowest N concentrations. As explained above, this is
because the condition that $V_B > kT/q$ is violated and the thermionic
emission theory does not hold unless this condition is true. The
fitting parameter for the argument of sinh, and the calculated value
of the grain size is shown in Table 4.4. The calculated grain size

I-V CURVE FIT PARAMETERS
VARIOUS TEMPERATURES

B VALUES
T= DEG. C

N2 DOSE	WAFER	T= 23	50	75	110
0	31	0.0510 *	0.0535 *	0.0600 *	0.0626 *
3.2E+15	25	0.0496 *	0.0477 *	0.0471 *	0.0470 *
1.0E+16	32	0.0370	0.0346	0.0321	0.0282
1.0E+16	23	0.0332	0.0308	0.0305	0.0291
3.2E+16	46	0.0289	0.0297	0.0276	0.0197
1.0E+17	49	0.0210	0.0158	0.0134	0.0153
1.0E+17	48	0.0192	0.0131	0.0123	0.0115
1.2E+17	1	0.0281	0.0172	0.0164	0.0166

CALCULATED GRAIN SIZE - ANGSTROMS

N2 DOSE	WAFER	23	50	75	110	AVG.
0	31	362 *	414 *	500 *	575 *	463
3.2E+15	25	352 *	369 *	393 *	431 *	386
1.0E+16	32	262	268	268	259	264
1.0E+16	23	236	238	254	267	249
3.2E+16	46	205	230	230	181	211
1.0E+17	49	149	122	112	140	131
1.0E+17	48	136	101	103	106	111
1.2E+17	1	199	133	137	152	155

1/kT (1/eV) =		39.19	35.91	33.33	30.29

* => POOR CURVE FIT

Table 4.4 I-V curve fit parameters - various temperatures.

is very consistent with that obtained by fitting I-V curves for various resistor lengths. A comparison of these values from Table 4.2 and 4.4 is shown in Table 4.5.

E. $1000^{\circ}C$ Anneal

Two wafers were annealed at $1000^{\circ}C$ in O_2 for 30 min to determine the effects of further heat treatment on the polysilicon resistors. Previous to this step all of the wafers have seen a nitrogen anneal at $900^{\circ}C$ for 30 min which activates the As implanted into the poly-silicon runners. The results of the resistivity measurements made at 5V on the 13.9 μm resistor are shown in Table 4.6. The resistivity for wafer 23, which had the 1 $E16/cm^2$ N implant, did not change significantly before and after the $1000^{\circ}C$ anneal. Wafer 48, which had the $1E17/cm^2$ N implant, showed a drop in the resistivity by a factor of 2.7.

The resistance versus length was measured at 5 V for both of these wafers and the curves are shown in Fig. 4.12. Both curves are fairly linear, although the 1E16 doped sample shows a fall off in resistance at the lower resistor lengths.

I-V curves were measured on both of these wafers before and after the $1000^{\circ}C$ anneal. The curves for wafer 48 show the normal sinh

GRAIN SIZE CALCULATIONS
COMPARISON - VARIOUS LENGTHS AND TEMPERATURES

SIZE IN ANGSTROMS

N2 DOSE	WAFER	VARIOUS LENGTHS AVG.	VARIOUS TEMPS AVG.
0	31	399	463
3.2E+15	25	365	386
1.0E+16	32	265	264
1.0E+16	23	329	249
3.2E+16	46	210	211
1.0E+17	49	135	131
1.0E+17	48	129	111
1.2E+17	1	161	155

Table 4.5 Grain size calculation comparison - various
lengths and temperatures.

Resistivity Change After 1000°C 30 min Anneal

	Wafer 23	Wafer 48
Implant dose (1/cm^2)	1 E16	1 E17
Doping density (1/cm^3)	3.92 E20	3.92 E21

Resistivity (Ohm-cm)

	Wafer 23	Wafer 48
Pre-1000 C		
Average:	5.44 E5	2.44 E4
Range:	5.34 - 5.72 E5	2.24 - 2.60 E4
Post-1000 C		
Average:	6.05 E5	9.00 E3
Range:	5.64 - 6.69 E5	8.37 - 9.39 E3

Table 4.6   Resistivity before and after 1000°C anneal.

RESISTANCE VS LENGTH, POST 1000°C
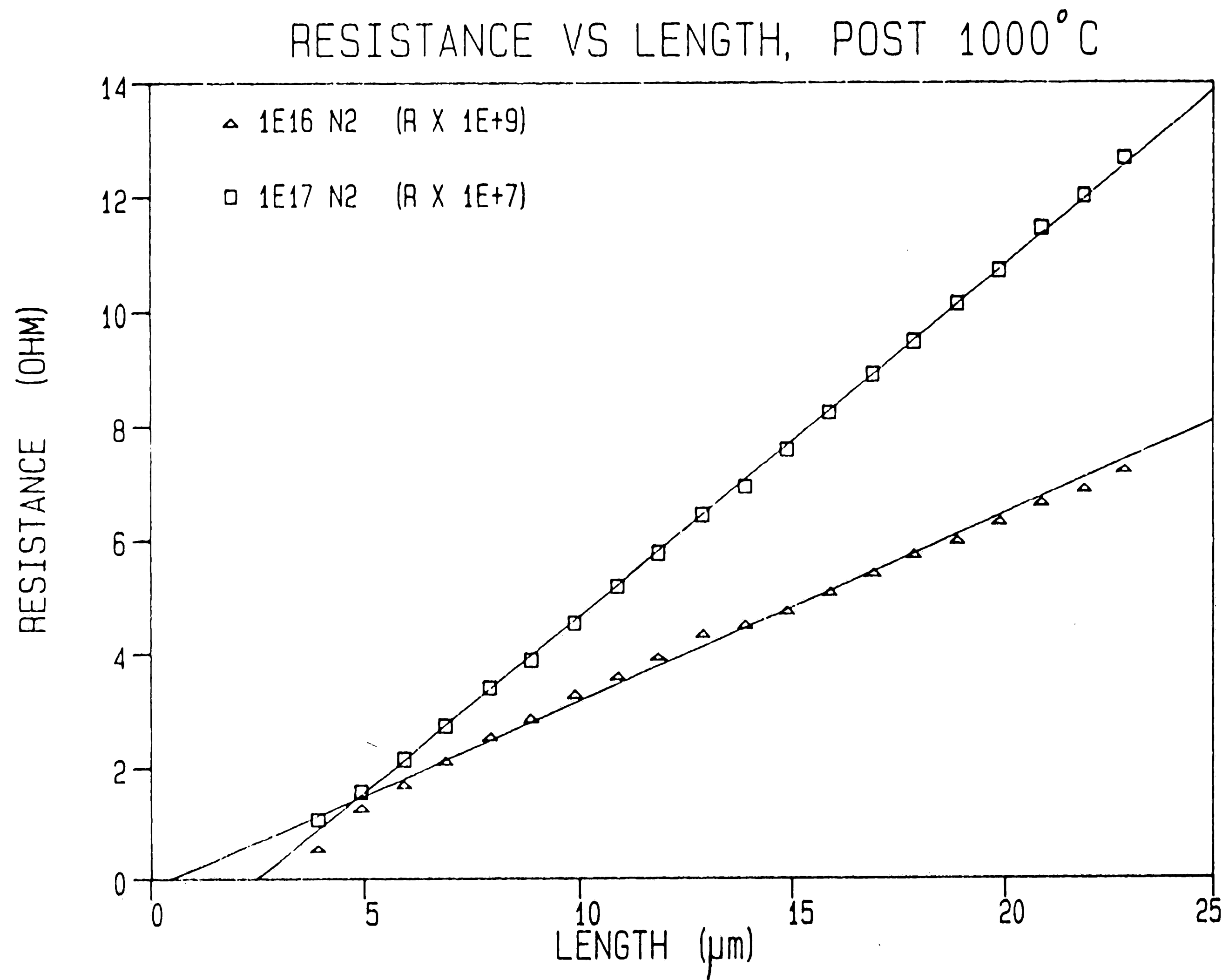
Fig. 4.12 Resistance vs length, post 1000°C anneal.

relationship before and after the anneal, but the curves for wafer 23 ($1E16/cm^2$) no longer show the sinh curve after the anneal. In Table 4.2, the calculated grain sizes for wafer 48 before and after the $1000^{o}C$ anneal are shown. The post anneal values are marked by "##". A comparison between the two shows a slight growth in the calculated grain size after anneal, and such growth due to heat treatments has been seen by many authors for normal dopants. Fig. 4.13 shows the measured I-V values as well as the sinh fit to the data.

The I-V characteristics for wafer 23 after the anneal show an unusual shape, see Fig. 4.14. There is a kink in the curve at about 15 V. The solid line is a sinh fit to the curve and one can see it is dominated by the higher values. This kink is seen for all resistor lengths but is less dominant for the longer resistors. It is possible that there is some As diffusion into the resistor, which will be discussed below. A hint of a problem with this sample is seen in Table 4.2 where the calculated value of the grain size for the 3.9 um resistor is twice that of the other resistor lengths, although the fit to the data is good. Also as noted, the R vs L curve of Fig. 4.12 shows a deviation at the small resistor lengths. These measurements were made at 5 V where the I-V curves are still well behaved.

Fig. 4.13 I-V curve, post 1000°C anneal, 1E17 N_2 dose.
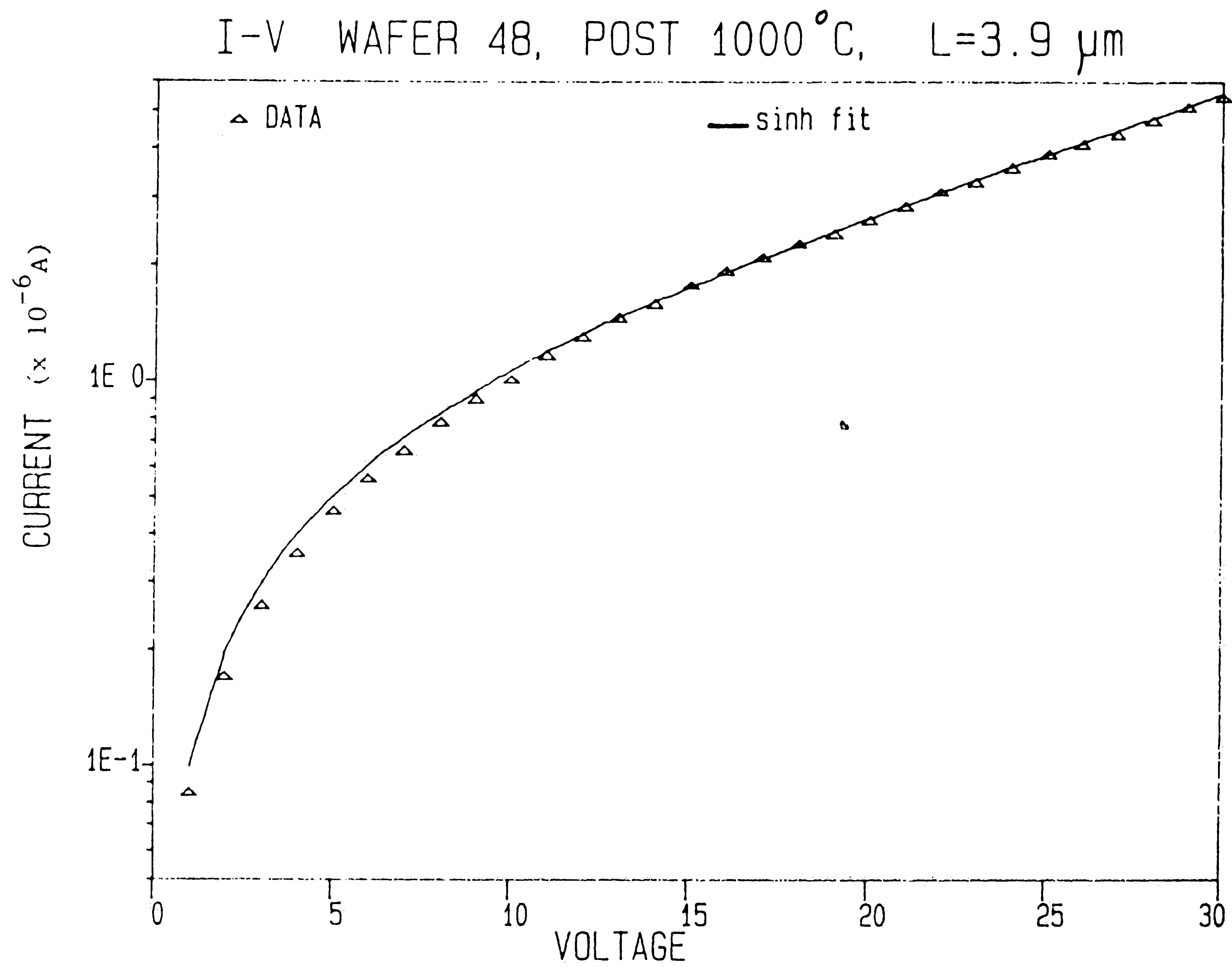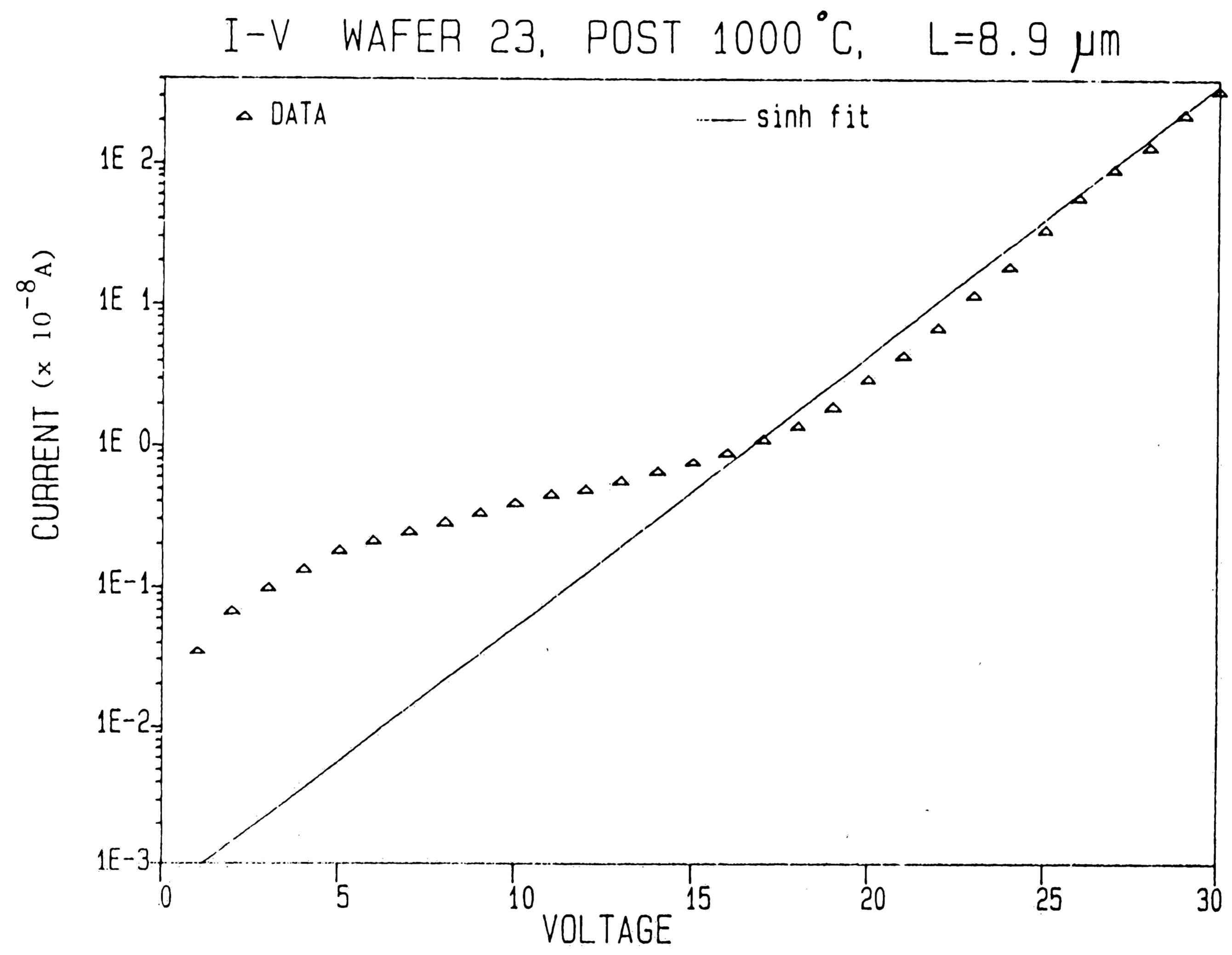
Fig. 4.14 I-V curve, post 1000°C anneal, 1E16 N_2 dose.

F. $1100^\circ C$ Anneal

Four wafers were further heat treated at $1100^\circ C$ in N_2 for 30 min.
Two of these wafers were already annealed at $1000^\circ C$ (wafers 23 and
48) and two had only seen the $900^\circ C$ anneal along with all of the
wafers. The resistors showed a significant decrease in resistance
after this anneal. The resistor values were now low enough that
when measuring them with 5 V applied, the current measured would
continually increase due to resistive heating. Therefore the resis-
tances were measure at 0.5 V applied where the current was stable,
rather than at the normal 5 V. The results of resistance measure-
ments for various resistor lengths are shown in Fig. 4.15. These
resistor values, when compared to Fig. 4.12, show a significant
change in behavior. For the long resistor length of 18.9 μm, the
value of resistance decreased by a factor of 12 for wafer 23 (1E16)
and 42 for wafer 48 (1E17). For the 8.9 μm long resistor the values
decreased by a factor of 4E5 and 4E2 for wafers 23 and 48
respectively. Similar results were obtained from the wafers which
had not seen the $1000^\circ C$ anneal previously.

The shape of the R vs L curves in Fig. 4.15 indicates that the
resistors below about 10 μm are shorted through by the diffusion of
As from the polysilicon contacts at either end. The reduction in
the resistance at the longer resistor lengths is probably due to a
small amount of As diffusion through the resistors, enough to have a

70

RESISTANCE VS LENGTH, POST 1100°C
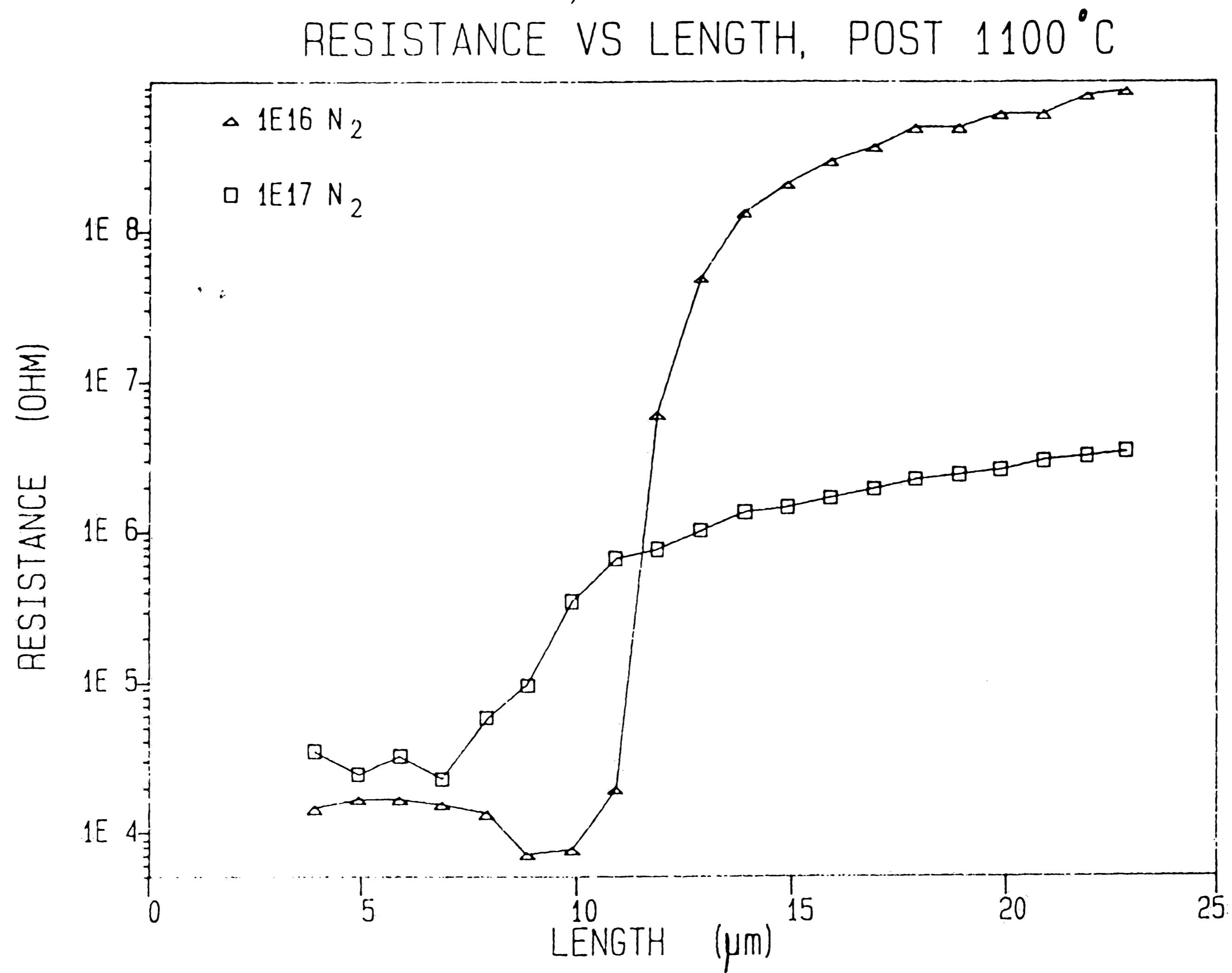
Fig. 4.15   Resistance vs length, post 1000°C anneal
(measured at 0.5V to reduce heating).

small effect, but not enough to short out the resistors.

The resistive heating in these resistors was large enough that meaningful I-V curves could not be obtained, even for the longer resistors. The measured current would drift upward with time at higher voltages.

G. Arsenic Diffusion

Each resistor is terminated at both ends by a junction with a heavily As doped polysilicon runner. During heat treatments, this As will diffuse into the resistor, with an effective shortening of the resistor length. As can be seen from the data after the 30 min $900^{\circ}C$ and $1000^{\circ}C$ anneals, the shortest resistor (3.9 um) is not shorted through, see Figs. 4.7, 4.8 and 4.12. After a 30 min. $1100^{\circ}C$ anneal, the shorter resistors are shorted, see Fig. 4.15.

A calculation of the diffusion of As in polysilicon can be made using published diffusion coefficients [30,52]. Data has also been collected on As diffusion in polysilicon by K. H. Lee in AT&T Bell Laboratories [53]. The results are summarized below in Table 4.7. The measurements of ref's [30,52] were made on the vertical diffusion of As in polysilicon, whereas those of K. H. Lee were measurements of the lateral diffusion of As, using a test structure like the one in this study.

As Diffusivities in Polysilicon

$$D = D_0 \exp(-E/kT)$$

$$\Delta L = 2x = 4\sqrt{Dt}\ \mathrm{erfc}^{-1}(C/C_s) = 10\sqrt{Dt}$$

Ref.	[53]	[52]	[30]
D_0 (cm^2/s)	0.128	0.63	8.6 E4
E (eV)	2.93	3.22	3.9
$\Delta \underline{L}$ (μm)			
T=900°C	0.78	0.40	5.24
T=1000°C	2.42	1.44	23.88
T=1100°C	6.40	4.16	87.08

Table 4.7 As diffusion in polysilicon, calculation.

73

The calculated resistor length change was done using the equation

$$\Delta L = 2x = 4\sqrt{Dt} \; erfc^{-1}(C/C_s)$$

where t is the diffusion time, C_s is the concentration in the diffusion source and C is the background concentration. It was assumed that the background concentration is the concentration required to see some conduction effects in polysilicon, and based on Fig. 2.3 and 2.5, a number of $1E17/cm^3$ was chosen. The diffusion source was polysilicon doped with a dose of $1E16/cm^2$, or $3.9E20/cm^3$. The value of $erfc^{-1}(C/C_s)$ is about 2.5, therefore

$$\Delta L = 10\sqrt{Dt}$$

One can see from Table 4.7, discounting the measurements of [30], that the shortest resistor (3.9 μm) would remain unshorted from the $1000^\circ C$ anneal, but after a $1100^\circ C$ anneal, resistors of length less than 4-6 μm would be shorted. This general trend is seen in the results of the heat treatments, although Fig. 4.15 shows that the N doping concentration also has an effect which is not accounted for in the simple diffusion theory. It is seen in single crystal Si that there is sometimes a strong effect on the diffusion due to the presence of other impurities, which is sometimes called the emitter push or pull effects. In this case there is a large concentration of N which may affect the As diffusion. The diffusion in polysilicon, which generally proceeds along the grain boundaries, is also dependent on the specific characteristics of each polysilicon film, and therefore strict comparisons with other

authors may be difficult.

H. Grain Size Measurements

A Transmission Electron Micrograph (TEM) was taken of a polysilicon resistor on wafer 46 (3E16/cm^2 N$_2$) to measure the grain size. The average size of the grains measured was about 1000 Å, with a large distribution around this measurement, with a sigma of about 50%. The actual TEM was not easy to interpret as many of the grains were indistinguishable.

The measured grain size of 1000 Å is a factor of 5 times larger than the calculated grain size of 210 Å. This discrepancy is common in the literature and is usually attributed to the large variation in grain sizes in a given sample. In ref. [20], the calculated grain size was 0.26-0.44 µm and the measured grain size varied from 1 µm at the surface to 0.1 µm at the Si-Sio$_2$ surface on a 3 um thick sample. In ref. [7], the calculated grain size is 1220 Å but the average grain size is 2400 Å, although the most frequently observed grain size was 1700 Å. The most frequently observed grain size generally gives the best agreement with the calculations. In this study, the TEM was not clear enough to distinguish many small grain sizes.

Polysilicon usually exhibits a large variation in grain sizes and

the actual meaning of the calculated grain size is questionable. As mentioned above, in ref. [9] the calculated grain size varies with doping levels and temperature although the physical grain size is unchanged. Regardless of the actual physical interpretation of the calculated grain size, this parameter does scale with the resistor length in almost all cases (see Table 4.2) and therefore provides a useful tool for designing resistors.

Chapter V

Conclusions

The results of these experiments show that nitrogen acts as a weak dopant in polycrystalline silicon and results in a much less abrupt change in resistivity with dopant concentration as compared with normal dopants of As, B and P. There is a variation in resistivity with N dopant concentration by a factor of 30 instead of 100,000 as measured on resistors with normal dopants. There is even an indication of an increase in resistivity at the highest N concentration of 4.7 E21 cm_a^{-3}. These results compare well with those obtained by H. Hayashi et al [18].

The actual cause of the reduced sensitivity of the resistivity to implant dose and the rise in resistance at the higher dose is unexplained, although it is speculated that it is due to the same effect that is seen in crystalline silicon, where a rise in resistivity at the higher implanted N doses occurs due to a reduction in free carriers [17]. This reduction in free carriers may be the same cause of the reduced resistivity range in polysilicon, although it is not well explained in crystalline Si yet. The formation of $Si_x N_x$ complexes is the most likely explanation.

The current, voltage and length characteristics behave similarly to

normally doped polysilicon resistors and follow the simple hyperbolic sine relationship of ref. [7] derived from the thermionic emission across grain boundaries. The sinh relationship does not fit the measurements at the highest temperature (150°C) and for the 2 lowest N concentrations because the conditions for thermionic emission are violated. The derived grain sizes using this relationship are approximately equal for different doping concentrations, except for the lowest concentrations where the conditions for thermionic emission are violated. The calculated grain sizes are about 5 times smaller than the grain sizes measured from electron micrographs. This discrepancy is common for normal dopants as well.

The resistance versus length measurements are approximately linear at 5 V, but at the lower doping concentrations show a negative intercept which may be explained by the built in resistance of the reverse biased junction between the heavily As doped polysilicon contacts and the almost intrinsic polysilicon resistor region [29].

The activation energy for different resistances remains at a higher value than for common dopants. The activation energy for N doped polysilicon ranges from half band gap to 0.36eV, whereas for normal dopants it ranges to as low as 0.06eV. [2,7,19]. Used as load elements, these resistors will better track the leakage current of a reverse biased p-n junction than normally doped polysilicon, which has a lower activation energy through much of its implant range.

Some of the nitrogen implanted resistors were annealed at $1000^{o}C$ and $1100^{o}C$ to determine the effects of further heat treatments that may be encountered during normal processing of integrated circuits. After the $1000^{o}C$ anneal, the $1E17/cm^2$ N implanted sample showed a drop in resistivity by a factor of 2.7 and the $1E16/cm^2$ sample did not significantly change, although the I-V characteristic of this sample changed significantly. After the $1100^{o}C$ anneal, both samples showed evidence of being shorted by the As diffusion from the heavily doped contacts.

Nitrogen implanted polysilicon resistors have a number of desirable attributes for the use in integrated circuit manufacturing. There is better control of the resistivity with implant dose and the activation energy is better matched to leakage currents. Unfortunately, the high doses required impose a serious limitation to the commercial manufacture of N doped resistors. The implant times in this study were up to 12 hours per wafer at the highest dose. These long times prohibit cost efficient manufacturing at this time. A higher current implant machine which would not overheat the samples would be needed, but no suitable facilities exist today.

The nitrogen implanted resistors have been characterized in terms of the data that would be needed for use in integrated circuit

manufacture, but there are some mechanisms wwhich are not understood theoretically. In order to better understand the conduction mechanisms of N implanted polysilicon, a measurement of the number of free carriers (perhaps using the Hall effect) versus the implant dose would be instructive. Also, measurements of higher implant doses would better characterize the rise in resistivity at the high end. Using a structure without As implanted polysilicon contacts at either end would allow higher temperature anneals to be performed without As diffusion problems and would give better data on these effects. The anneal could be performed first and then aluminum contacts could be placed on the ends of the resistors. Other analytical techniques may also be applied to study the bonding of N to Si in these samples. These additional studies would help to better understand the theoretical conduction mechanisms.

REFERENCES

1   J. M. Andrews, J. Electronic Mat. $\underline{8}$, 227 (1979).

2   G. Baccarani, B. Ricco and G. Spandini, J. Appl. Phys. $\underline{49}$, 5565 (1978).

3   A. L. Fripp, J. Appl. Phys. $\underline{46}$, 1240 (1975).

4   J. Y. M. Lee and I. C. Cheng, J. Appl. Phys. $\underline{53}$, 490 (1982).

5   N. C. C. Lu, L. Gerzberg and J. D. Meindl, IEEE Electron Dev. Lett. $\underline{EDL-1}$, 38 (1980).

6   N. C. C. Lu, L. Gerzberg, C. Y. Lu and J. D. Meindl, IEEE Electron Dev. Lett. $\underline{EDL-2}$, 95 (1981).

7   N. C. C. Lu, L. Gerzberg, C. Y. Lu and J. D. Meindl, IEEE Trans. Electron Dev. $\underline{ED-28}$, 818 (1981).

8   N. C. C. Lu, L. Gerzberg, and J. D. Meindl, IEEE Trans. Electron Dev. $\underline{ED-29}$, 682 (1982).

9   N. C. C. Lu, C. Y. Lu, M. K. Lee and G. Chang, IEEE Tech. Dig., Int. Electron Device Meet., 706 (1982).

10   N. C. C. Lu, L. Gerzberg, C. Y. Lu and J. D. Meindl, IEEE Trans. Electron Dev. $\underline{ED-30}$, 137 (1983).

11   M. M. Mandurah, K. C. Saraswat and T. I. Kamins, IEEE Trans. Electron Dev. $\underline{ED-28}$, 1163 and 1171 (1981).

12   J. C. North, A. C. Adam and G. F. Richards, in Quick Reference Manual for Silicon Integrated Circuit Technology, edited by W. E. Beadle, J. C. C. Tsai, R. D. Plummer (Wiley, New York),

81

pp. 7-61 to 7-69 (1985).

13   Y. Saito, I. Mizushima and H. Kuwano, J. Appl. Phys. 57, 2010
      (1985).

14   C. H. Seager and T. G. Castner, J. Appl. Phys. 49, 3879
      (1978).

15   J. Y. W. Seto, J. Appl. Phys. 46, 5247 (1975).

16   C.-Y. Wu and W.-D. Ken, Solid-State Electron. 26, 675 (1983).

17   P. V. Pavlov, E. I. Zorin, D. I. Tetelbaum and A. F. Khokholv,
      Phys. Stat. Sol. a35, 11 (1976).

18   H. Hayashi, H. Yamoto, and T. Oshima, The Electrochem. Soc.
      Extended Abstracts 83-1, 645 (1983).

19   D. M. Kim, A. N. Khondker, R. R. Shah and D. L. Crosthwait,
      Jr., IEEE Electron Dev. Lett. EDL-3, 141 (1982).

20   G. J. Korsh and R. S. Muller, Solid-State Electron. 21, 1045
      (1978).

21   T. Matsushita et al., Proc. 7th Conf. Solid State Devices,
      Tokyo, 1975; Japan. J. Appl. Phys. 15 (1976) Suppl., p.35.

22   T. Matsushita et al., IEEE Trans. Electron Dev. ED-23, 826
      (1976).

23   H. Mochizuki et al., Proc. 7th Conf. Solid State Devices,
      Tokyo, 1975; Japan. J. Appl. Phys. 15 (1976) Suppl., p.41.

24   J. T. McGinn and A. M. Goodman, Appl. Phys. Lett. 34, 601
      (1979).

25   T. I. Kamins, M. M. Mandurah and K. C. Saraswat, J.

Electrochem. Soc., Solid-State Sci. and Tech. 125, 927 (1978).

26   M. M. Mandurah et al., J. Appl. Phys. 51, 5755 (1980).

27   E. Loh, J. Appl. Phys. 54, 4463 (1983).

28   S. M. Sze, Physics of Semiconductor Devices, Wiley

Interscience, New York (1981) p. 258.

29   J. E. Mahan, D. S. Newman and M. R. Gulett, IEEE Trans.

Electron Dev. ED-30, 45 (1983).

30   B. Swaminathan et al., Appl. Phys. Lett. 40, 795 (1982).

31   Y. Wada and S. Nishimatsu, J. Electrochem. Soc., Solid-State

Sci. and Tech. 125, 1499 (1978).

32   T. Nakashita, K. Kohno, T. Imura and Y. Osaka, Japan. J. Appl.

Phys. 23, 1547 (1984).

33   P. C. Mathur, et al., J. Appl. Phys. 54, 3913 (1983).

34   L. Mei, M. Rivier, Y. Kwart and R. W. Dutton, in Proc. 4th

Int. Symp. Silicon Materials Sci. and Technol. 81-5, 1007

(1981).

35   C. P. Ho et al., IEEE Trans. Electron Dev. ED-30, 1438 (1983).

36   W. Kaiser and C. D. Thurmond, J. Appl. Phys. 30, 427 (1959).

37   K. Sumino, I. Yonenaga, M. Imai and T. Abe, J. Appl. Phys. 54,

5016 (1983).

38   H. Niu, T. Matsuda, K. Yamauchi and M. Takai, Appl. Phys.

Lett. 21, 423 (1972).

39   P. V. Pavlov, E. I. Zorin, D. I.Tetel'baum and Y. S. Popv,

Soviet Physics - Doklady 10, 786 (1966).

40   E. I. Zorin, P. V. Pavlov and D. I. Tetel'baum, Soviet Physics - Semiconductors 2, 111 (1968).

41   K. L. Brower, Phys. Rev. Lett. 44, 1627 (1980).

42   K. L. Brower, Inst. Phys. Conf. Ser. 59, 491 (1981).

43   K. L. Brower, Phys. Rev. B 26, 6040 (1982).

44   P. P. Pronko, J. B. Mitchell and J. Shewchun, in Ion Implantation in Semiconductors, Proceed. of II. Intern. Conf. on Ion Implan. in Semicon., Physics and Techn., 1971, edited by I. Ruge and J. Graul, Springer-Verlag, VIII.8, 495 (1971).

45   J. B. Mitchell et al., J. Appl. Phys. 46, 332 and 335 (1975).

46   T. P. Smith et al., J. Appl. Phys. 58, 193 (1985).

47   Y. Yatsurugi, N. Akiyama, Y Endo and T. Nozaki, J. Electrochem. Soc., Solid-State Sci. and Tech. 120, 975 (1973).

48   C. H. Seager and D. S. Ginley, Appl. Phys. Lett. 34, 337 (1979).

49   G. Sasaki, M. Kondo, S. Fujita and A. Sasaki, Japan. J. Appl. Phys. 21, L377 (1982).

50   T. Makino and H. Nakamura, Appl. Phys. Lett. 35, 551 (1979).

51   J. C. North, A. C. Adam and G. F. Richards, in Quick Reference Manual for Silicon Integrated Circuit Technology, edited by W. E. Beadle, J. C. C. Tsai, R. D. Plummer (Wiley, New York), pp.7-68, 7-69 (1985).

52   K. Tsukamoto, Y. Akasaka and K. Horie, J. Appl. Phys. 48, 1815 (1977).

53   K. H. Lee and B. R. Jones - private communication.

54   Quick Reference Manual for Silicon Integrated Circuit Tech-
      nology, edited by W. E. Beadle, J. C. C. Tsai, R. D. Plummer
      (Wiley, New York), pg. 2.71 (1985).

55   Quick Reference Manual for Silicon Integrated Circuit Tech-
      nology, edited by W. E. Beadle, J. C. C. Tsai, R. D. Plummer
      (Wiley, New York), pp. 6.31 and 6.32 (1985).

VITA

Carl Alexis Peridier was born on May 1, 1953 in Alexandria Virginia to Mildred Pauline and Paul Herman Peridier. He received his Bachelor of Science in Physics from the University of Maryland, College Park, in 1975 graduating with high honors in physics and general high honors. In 1978 he graduated with a Master of Science Degree in Physics from the Massachusetts Institute of Technology, with a thesis on intermediate energy nuclear physics. Mr. Peridier has done research at the Cyclotron accelerator at the University of Maryland, the Tandem Van de Graaff accelerator at Brookhaven National Laboratory and the Bates Linear Accelerator at M.I.T. He has co-authored many articles on nuclear physics and authored "The ^{3}He(γ,2p)n Reaction for E_γ = 80-170 MeV" in Zeitschrift fur Physik A - Atoms and Nuclei (1983). Mr. Peridier is a member of the honorary fraternities Sigma-Pi-Sigma, Pi-Mu-Epsilon and Phi-Kappa-Phi.

Since 1978, Mr. Peridier has been employed by AT&T Technologies in Allentown Pennsylvania, where his responsibilities have been primarily associated with MOS integrated circuit manufacture.